Steady-state/Hopf interaction in the van der Pol oscillator with delayed feedback

Jason Bramburger

Thesis submitted to the Faculty of Graduate and Postdoctoral Studies
in partial fulfillment of the requirements for the degree of Master of Science in Mathematics [1]

Department of Mathematics and Statistics
Faculty of Science
University of Ottawa

[1]The M.Sc. program is a joint program with Carleton University, administered by the Ottawa-Carleton Institute of Mathematics and Statistics

Abstract

In this thesis we consider the traditional Van der Pol Oscillator with a forcing dependent on a delay in feedback. The delay is taken to be a nonlinear function of both position and velocity which gives rise to many different types of bifurcations. In particular, we study the Zero-Hopf bifurcation that takes place at certain parameter values using methods of centre manifold reduction of DDEs and normal form theory. We present numerical simulations that have been accurately predicted by the phase portraits in the Zero-Hopf bifurcation to confirm our numerical results and provide a physical understanding of the oscillator with the delay in feedback.

Acknowledgements

Thank you to my supervisors Dr. Victor Leblanc and Dr. Benoit Dionne for their guidance and support along the way and to the University of Ottawa for this opportunity to further my education.

Dedication

This work is dedicated to my family for all of their support along the way.

Contents

List of Figures

Chapter 1

Introduction

In 1920, while working as an engineer, Balthasar van der Pol published *A theory of the amplitude of free and forced triode vibrations* [15] in which he presented the oscillator that bears his name, given by

$$\ddot{x}(t) + \varepsilon(x^2(t) - 1)\dot{x}(t) + x(t) = f(t), \tag{1.1}$$

where $\varepsilon > 0$. Originally equation (1.1) was a model for an electrical circuit with a triode valve, and it has evolved into one of the most celebrated equations in the study of nonlinear dynamics.

Van der Pol found that in the unforced system (when $f \equiv 0$) the trivial equilibrium point is unstable and the system contains a stable oscillation for all values of ε. He also explored the effect of a periodic forcing on his oscillator, which for example, can be given by

$$\ddot{x}(t) + \varepsilon(x^2(t) - 1)\dot{x}(t) + x(t) = A\cos\left(\frac{2\pi t}{T}\right). \tag{1.2}$$

Upon adding this periodic forcing, van der Pol found that much more complicated phenomena could arise in the system. As the study of nonlinear differential equations has progressed, it has become known that the system exhibits chaotic behaviour when the nonlinearity becomes larger (i.e. $\varepsilon = 8.53$). Because of the many different

examples of nonlinear dynamics that occur in the system, the van der Pol oscillator has become a recurring example in modern mathematics.

The van der Pol oscillator has become synonymous with modern systems that exhibit limit cycle oscillations in many far reaching branches of the physical sciences. Kaplan et al. provide a simple example of a biological application of the van der Pol oscillator to the dynamics of the heart [9], and the FitzHugh-Nagumo model is a modified form of the oscillator that has direct applications to neurones in the brain. On the larger scale, Cartwright et al. showed that the van der Pol oscillator can be used to model earthquake faults with viscous friction [3]. All of these applications and many more make the van der Pol oscillator one of the most widely celebrated differential equations in mathematics and one that is just as relevant today as the day that van der Pol himself presented the equation.

Despite all of these applications of the van der Pol oscillator, it wasn't until around the start of the twenty-first century, almost eighty years after van der Pol introduced his equation, that mathematicians began to experiment with the effect of delays on the equation. Delay differential equations have proven to be useful in many physical problems ranging from the study of neural networks to the cutting of metal (see [13, 14]). For this reason, it is especially useful to study the effect of delays on one of the most famous nonlinear differential equations in all of mathematics to observe the power that a lag in communication can have over a dynamical system.

Atay [2] studied the equation

$$\ddot{x}(t) + \varepsilon(x^2(t) - 1)\dot{x}(t) + x(t) = \varepsilon k x(t - \tau), \tag{1.3}$$

where $\tau > 0$ is a delay, and found that the stability of the limit cycle present in the system now depended on the amount of delay applied to the system. A similar study was presented by Oliveira [12], in which they added delays in the nonlinear terms of the unforced system, and found that periodic solutions still existed under certain conditions. Both of these studies confirmed that the effect of adding a delay

to the equation can vastly affect the behaviour of the system and provide us with an outcome not easily predicted upon first inspection.

It was Wei and Jiang [16, 17] who considered the forcing on the equation as a nonlinear function of the delay in position, $x(t)$, given by

$$\ddot{x}(t) + \varepsilon(x^2(t) - 1)\dot{x}(t) + x(t) = g(x(t - \tau)). \tag{1.4}$$

They found that under certain conditions single, double and triple zero eigenvalues were possible as well as a purely imaginary pair with a zero eigenvalue. The cases of the single and double zero eigenvalues were presented in [17] and [8], respectively, with full details of the nature of their respective bifurcations. Later, Wu and Wang [19] undertook the bifurcation analysis of the purely imaginary pair and the zero eigenvalue to find that a Zero-Hopf bifurcation was occurring. They found that under certain conditions only two of the four possible bifurcation diagrams of the Zero-Hopf bifurcation were possible due to restrictions put in place by the initial assumptions on the nonlinear forcing.

In this thesis we consider the van der Pol oscillator with general nonlinear delayed damping,

$$\ddot{x}(t) + \varepsilon(x^2(t) - 1)\dot{x}(t) + x(t) = g(\dot{x}(t - \tau), x(t - \tau)), \tag{1.5}$$

where g $\in C^3$, $g(0, 0) = 0$, $g_{\dot{x}}(0, 0) = a$ and $g_x(0, 0) = b$, and work to understand its dynamics. This allows us to consider the work of Wei and Jiang as a special case of equation (1.5), and as in their work, we find all bifurcations are again possible with the added possibility of a quadruple zero bifurcation. This thesis will concentrate on the Zero-Hopf bifurcation taking place, and we will see that the added delay in the velocity has now allowed us to explore all possible bifurcation diagrams predicted for the Zero-Hopf bifurcation. We will use methods of normal form reduction on the centre manifold to effectively study the dynamics of the system near the bifurcation. This will therefore allow us to observe the dynamics of the Zero-Hopf bifurcation as it occurs on the centre manifold.

We begin our study with an in-depth analysis of the characteristic equation of equation (1.5) and provide the necessary conditions under which each distinct bifurcation in the system will be present. After summarizing the analysis of the Zero-Hopf bifurcation and the centre manifold reduction for DDEs, we work to reduce our infinite-dimensional system to a reduced three-dimensional system on the centre manifold. Upon finding the equivalent system on the centre manifold, we work to connect ourselves with the normal form given by the Zero-Hopf bifurcation and therefore offer a complete unfolding of the system using the bifurcation parameters. Upon completing our analysis of the system we use computational tools that allow us to numerically simulate the system and confirm our theoretical results. Please note that Chapters 3 and 4 are contain known results and provide the foundation for many of the main concepts to be used later. These concepts are applied to equation 1.5 in Chapters 2, 5, 6, and 7 where the results given are the independent work of the author.

Chapter 2

The Characteristic Equation

In this chapter, we will work to identify the eigenvalues of equation (1.5) and, more specifically, the conditions that lead to eigenvalues on the imaginary axis. Upon linearizing around the solution $x(t) = 0$, we obtain

$$\ddot{x}(t) - \varepsilon\dot{x}(t) + x(t) = a\dot{x}(t-\tau) + bx(t-\tau). \tag{2.1}$$

Now, substituting the ansatz $x(t) = e^{\lambda t}$ into (2.1), where λ is a complex parameter, we find the associated characteristic equation to be

$$\Delta(\lambda, \tau) := \lambda^2 - \varepsilon\lambda + 1 - (a\lambda + b)e^{-\lambda\tau} = 0. \tag{2.2}$$

This brings us to the following theorem about the roots of equation (2.2).

Theorem 2.1. *Suppose that $b = 1$ is satisfied. Then*

(i) $\lambda = 0$ *is a single root to Eq.* (2.2) *when* $\tau \neq \varepsilon + a$*;*

(ii) $\lambda = 0$ *is a double root to Eq.* (2.2) *when* $\tau = \varepsilon + a$ *and* $\varepsilon^2 - a^2 \neq 2$*;*

(iii) $\lambda = 0$ *is a triple root to Eq.* (2.2) *when* $\tau = \varepsilon + a$*,* $\varepsilon^2 - a^2 = 2$ *and* $\varepsilon \neq \varepsilon_0 \approx 1.632993162$*;*

(iv) $\lambda = 0$ *is a quadruple root to Eq.* (2.2) *when* $\tau = \varepsilon + a$*,* $\varepsilon^2 - a^2 = 2$ *and* $\varepsilon = \varepsilon_0$*;*

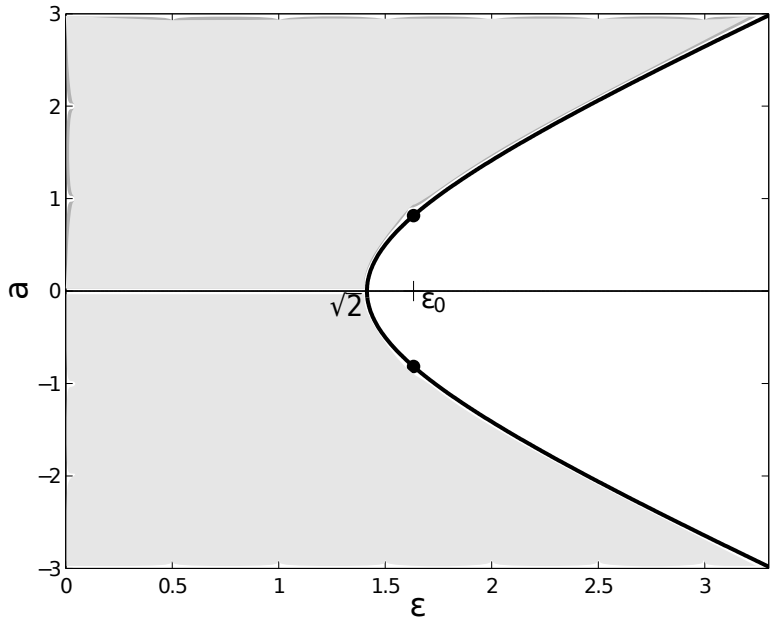

Figure 2.1: Diagram of the (ε, a)-plane. The shaded area shows where complex conjugate roots of the characteristic equation occur.

(v) If $\tau = \tau_0 \neq \varepsilon + a$ and $\varepsilon^2 - a^2 < 2$, Eq. (2.2) has a simple zero root and a pair of purely imaginary roots $\lambda = \pm i\omega_0$. Here ω_0 and τ_0 are defined by

$$\omega_0 = \sqrt{2 - \varepsilon^2 + a^2}, \qquad \tau_0 = \frac{1}{\omega_0} \arccos\left(\frac{1 - (1 + \varepsilon a)\omega_0^2}{a^2\omega_0^2 + 1}\right).$$

Proof: Immediately we see that $\lambda = 0$ is a root of Eq. (2.2) if and only if $b = 1$. Substituting $b = 1$ into $\Delta(\lambda, \tau)$ and differentiating with respect to λ, we get

$$\frac{d\Delta(\lambda, \tau)}{d\lambda} = 2\lambda - \varepsilon - ae^{-\lambda\tau} + a\lambda\tau e^{-\lambda\tau} + \tau e^{-\lambda\tau}. \tag{2.3}$$

Hence when $\lambda = 0$ Eq. (2.3) is 0 if and only if $\tau = \varepsilon + a$, and the conclusion of (i) follows.

By differentiating Eq. (2.3), we obtain

$$\left.\frac{d^2\Delta(\lambda, \tau)}{d\lambda^2}\right|_{\tau=\varepsilon+a} = 2 - (\varepsilon^2 - a^2)e^{-\lambda(\varepsilon+a)} - a\lambda(\varepsilon + a)^2 e^{-\lambda(\varepsilon+a)}. \tag{2.4}$$

Again setting $\lambda = 0$ Eq. (2.4) is 0 if and only if $\varepsilon^2 - a^2 = 2$, and hence the conclusion of (ii) follows.

From Eq. (2.4), we find that

$$\left.\frac{d^3\Delta(0,\tau)}{d\lambda^3}\right|_{\tau=\varepsilon+a,\varepsilon^2-a^2=2,\lambda=0} = 6\varepsilon - 2\varepsilon^3 \pm 2(\varepsilon^2-2)\sqrt{\varepsilon^2-2}. \tag{2.5}$$

Eq. (2.5) has only one positive root, denoted ε_0, and the conclusion of (iii) follows.

From Eq. (2.5), we get that $d^4\Delta(0,\tau)/d\lambda^4|_{\tau=\varepsilon_0+a,\varepsilon_0^2+a^2=2} \neq 0$ for either choice of a, which gives the conclusion of (iv).

By taking $\lambda = i\omega$ ($\omega > 0$) in (2.2), when $b = 1$ we get

$$1 - \omega^2 = \cos(\omega\tau) + a\omega\sin(\omega\tau) \quad \text{and} \quad -\varepsilon\omega = a\omega\cos(\omega\tau) - \sin(\omega\tau). \tag{2.6}$$

Squaring and adding the above equations gives $\omega^2[\omega^2 + (\varepsilon^2 - 2 - a^2)] = 0$. Denote the positive, nonzero root of this equation ω_0. Similarly, the expression for τ_0 can be obtained by a simple manipulation on the equations in (2.6) to isolate $\cos(\omega\tau)$, and hence the conclusion of (v) follows. ∎

The first thing that we should note after considering this theorem is that the addition of the parameter a has opened up the possibility of a quadruple zero eigenvalue, something that is unattainable in Jiang and Wei's work. The locations of the ε and a pairs which give the quadruple zero eigenvalue are shown by the two points along the line $\varepsilon^2 - a^2 = 2$ in Figure 2.1. The figure shows the particular regions in the (ε, a)-plane at which each of the multiplicities of the zero eigenvalue can be obtained. By considering delays in both the position and the velocity of the object, we have effectively allowed for the possibility of more complicated dynamics in the original system proposed by Jiang and Wei. Although the existence of the quadruple zero eigenvalue is interesting, few, if any, theoretical results are known about this bifurcation. Consequently, an analysis of this singularity is beyond the scope of this thesis.

Furthermore, where cases (i) and (ii) correspond to codimension one and two bifurcations respectively, cases (iii) and (iv) are codimension three and four respectively, making the analysis increasingly more difficult as the codimension rises.

The grey region bounded by $\varepsilon \geq 0$ and $\varepsilon^2 - a^2 < 2$ gives the location of the pairs (ε, a) such that equation (2.2) has a pair of complex conjugate roots on the imaginary axis, as well as a zero root. This will be the area that will be focused upon for the remainder of the work presented. We will see in the coming chapters that under the conditions given by Theorem 2.1(v) a Zero-Hopf Bifurcation (a codimension two bifurcation) is occurring and how the addition of a delay in velocity will yield results generalizing those presented by Wang and Wu in [19].

Chapter 3

A Pure Imaginary Pair and a Simple Zero Eigenvalue

Here we will use the methods from [6] and [10] to provide a partial theoretical analysis of the Zero-Hopf bifurcation. This particular bifurcation was first studied by W. F. Langford in his 1979 paper *Periodic and steady-state mode interactions lead to tori* [11], where he completely analyzed the local codimension two bifurcation that occurs when we have a purely imaginary pair and a simple zero eigenvalue. This chapter will provide a brief overview of his work to provide us with some expectations for the bifurcation that is occurring in the unfolding of equation (1.5).

Using the method of normal form reduction, Guckenheimer and Holmes tell us in [6] that the normal form of a differential equation with linear part

$$\begin{pmatrix} \dot{x} \\ \dot{y} \\ \dot{z} \end{pmatrix} = \begin{bmatrix} 0 & -\omega & 0 \\ \omega & 0 & 0 \\ 0 & 0 & 0 \end{bmatrix} \begin{pmatrix} x \\ y \\ z \end{pmatrix}, \tag{3.1}$$

can be written in cylindrical coordinates as

$$\begin{cases} \dot{r} = a_1 rz + a_2 r^3 + a_3 rz^2 + \mathcal{O}(|r,z|^4), \\ \dot{z} = b_1 r^2 + b_2 z^2 + b_3 r^2 z + b_4 z^3 + \mathcal{O}(|r,z|^4) \\ \dot{\theta} = \omega + \mathcal{O}(|r,z|^2), \end{cases} \tag{3.2}$$

by applying the change of coordinates $x = r\sin(\theta)$, $y = r\cos(\theta)$, and $z = z$, where $\mathcal{O}(|r,z|^k)$ denotes terms of the kth degree and higher in r and z. Conveniently, the normal form contains no θ-dependent terms for large k, and therefore the azimuthal component in (3.2) can be decoupled, leaving us with a degenerate two dimensional vector field.

Truncating (3.2) at $\mathcal{O}(|r,z|^2)$ and eliminating the azimuthal component, we get

$$\begin{cases} \dot{r} = a_1 rz, \\ \dot{z} = b_1 r^2 + b_2 z^2, \end{cases} \tag{3.3}$$

in which we assume that $a_1, b_1, b_2 \neq 0$. By applying the rescaling $\bar{r} = -\sqrt{|b_1 b_2|}$, $\bar{z} = -b_2 z$ we can decrease the number of coefficients and obtain the equivalent system

$$\begin{cases} \dot{r} = arz, \\ \dot{z} = br^2 - z^2, \end{cases} \tag{3.4}$$

where $a = -a_1/b_2$ is assumed to be nonzero and $b = \pm 1$.

Guckenheimer and Holmes [6] give six distinct topological types for this normal form, which are given in Figure 3.1. They note that the cases $b = +1$, $a < 0$ can be grouped together since their unfoldings are nearly identical, which is also the case when $b = -1$, $a < 0$.

As we work to obtain the universal unfolding of the normal form (3.2), we will add the two-parameter linear part

$$\begin{pmatrix} \mu_1 x \\ \mu_1 y \\ \mu_2 \end{pmatrix}, \tag{3.5}$$

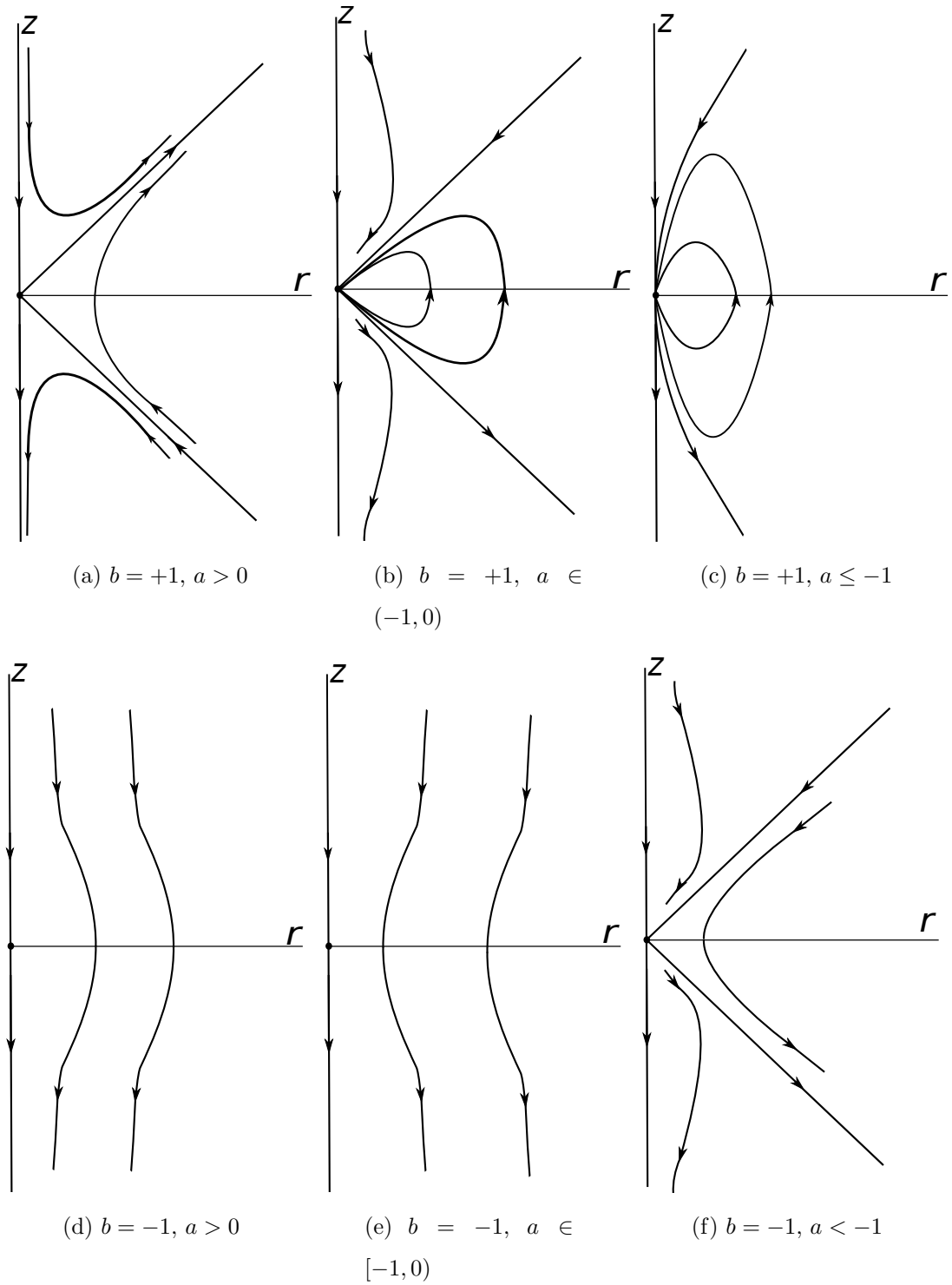

(a) $b = +1$, $a > 0$ (b) $b = +1$, $a \in (-1, 0)$ (c) $b = +1$, $a \leq -1$

(d) $b = -1$, $a > 0$ (e) $b = -1$, $a \in [-1, 0)$ (f) $b = -1$, $a < -1$

Figure 3.1: The six topological types for the normal form given in (3.4).

which [6] tells us will now provide all possible state perturbations of the fixed points up to a topological conjucacy. In terms of the planar system (3.4), we get

$$\begin{cases} \dot{r} = \mu_1 r + arz, \\ \dot{z} = \mu_2 + br^2 - z^2. \end{cases} \tag{3.6}$$

This system has fixed points at

$$(r, z) = (0, \pm\sqrt{\mu_2}), \tag{3.7}$$

for $\mu_2 \geq 0$, and

$$(r, z) = \left(\sqrt{\frac{1}{b}\left(\frac{\mu_1^2}{a^2} - \mu_2\right)}, -\frac{\mu_1}{a}\right), \tag{3.8}$$

for $\mu_1^2 \geq a^2\mu_2$ if $b = +1$ and $\mu_1^2 \leq a^2\mu_2$ if $b = -1$, and the linearized system has matrix

$$\begin{bmatrix} \mu_1 + az & ar \\ 2br & -2z \end{bmatrix}. \tag{3.9}$$

We now turn to the case when $b = +1$ and $a > 0$, which corresponds to Figure 3.1*a*. At the fixed points $(r, z) = (0, \pm\sqrt{\mu_2})$, matrix (3.9) is diagonal and takes the form

$$\begin{bmatrix} \mu_1 \pm a\sqrt{\mu_2} & 0 \\ 0 & \mp 2\sqrt{\mu_2} \end{bmatrix}. \tag{3.10}$$

Therefore, when $\mu_2 > 0$, we see that the fixed point $(0, \sqrt{\mu_2})$ is a sink provided $-a\sqrt{\mu_2} > \mu_1$, and similarly, $(0, -\sqrt{\mu_2})$ is a source provided $\mu_1 > a\sqrt{\mu_2}$; outside of their respective regions each point becomes a saddle.

This tells us that crossing the line $\mu_2 = 0$ for $\mu_1 \neq 0$, a saddle-node bifurcation is occurring on the invariant line $r = 0$. Similarly, crossing $\mu_2 = \mu_1^2/a^2$ with μ_2 decreasing for $\mu_1 \neq 0$, pitchfork bifurcations occur from the fixed point $(r, z) = (0, +\sqrt{\mu_2})$ if $\mu_1 < 0$ and $(0, -\sqrt{\mu_2})$ if $\mu_1 > 0$ (since we are only interested in the case when $r > 0$). On the curve $\mu_2 = \mu_1^2/a^2$ the fixed points in which these pitchfork bifurcations are occurring have a zero eigenvalue and are therefore referred to as degenerate fixed points.

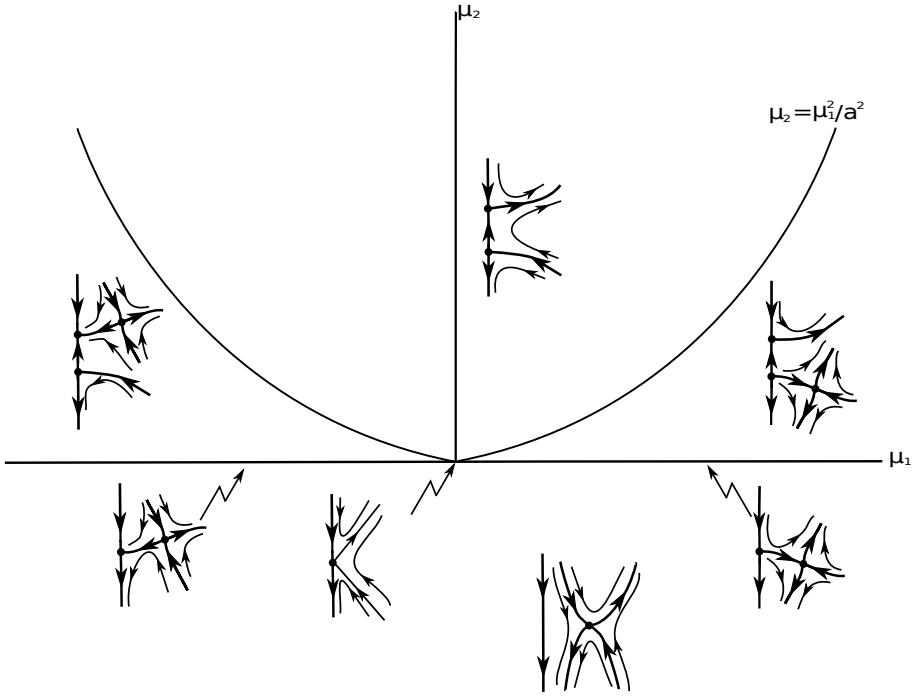

Figure 3.2: The universal unfolding when $b = +1$, $a > 0$. On the curve $\mu_2 = \mu_1^2/a^2$ phase portraits are homeomorphic to those above the curve, but the lower saddle is degenerate if $\mu_1 > 0$ and the upper saddle is degenerate if $\mu_1 < 0$.

Using matrix (3.9), we see that the fixed point $(r, z) = (\sqrt{\mu_1^2/a^2 - \mu_2}, -\mu_1/a)$ is a saddle for all $\mu_2 < \mu_1^2/a^2$, and we have now completed our study of this particular case of the Zero-Hopf bifurcation. The complete unfolding in the (μ_1, μ_2) plane is given in Figure 3.2 along with the associated phase portraits.

We should note that all phase portraits are in cylindrical coordinates and therefore the trajectories have a different meaning in the original three dimensional system. That is, all trivial fixed points, given when $r = 0$, relate to a fixed point in the original system, but nontrivial fixed points relate to a limit cycle corresponding to a slice of a cylinder. Furthermore, limit cycles in cylindrical coordinates will relate to an invariant torus in the regular coordinate systems. Similarly, a heteroclinic orbit's trajectory will follow along a sphere with poles at the trivial fixed points. It is very important to understand the connection between these phase diagrams to ensure that we can draw

immediate conclusions from the system in the three-dimensional Euclidean system.

We now move to the case when $b = +1$ and $a < 0$, whose origin on the bifurcation diagram is shown in Figures 3.1*b* and 3.1*c*. Using computations similar to the previous case, we find that the fixed point $(0, +\sqrt{\mu_2})$ is a saddle point provided $\mu_1 > -a\sqrt{\mu_2}$, and is otherwise a sink. Furthermore, the point $(0, -\sqrt{\mu_2})$ is a saddle point provided $a\sqrt{\mu_2} > \mu_1$, and is otherwise a source. As before, we have that saddle-node and pitchfork bifurcations are occurring on $\mu_2 = 0$ and $\mu_2 = \mu_1^2/a^2$, respectively.

Now we will see that the behaviour of the third fixed point, given by $(r, z) = (\sqrt{\mu_1^2/a^2 - \mu_2}, -\mu_1/a)$, is very different in this case. The eigenvalues of the linearized matrix (3.9) at this fixed point are given by

$$\lambda_{1,2} = \frac{\mu_1}{a} \pm \sqrt{\frac{\mu_1^2}{a^2} + \frac{2}{a}(\mu_1^2 - a^2\mu_2)}, \tag{3.11}$$

and therefore it is a sink for $\mu_1 > 0$ and a source for $\mu_1 < 0$. As we cross $\mu_1 = 0$ for $\mu_2 < 0$ we see that a Hopf bifurcation is occurring. Interestingly, when $\mu_1 = 0$, the system becomes

$$\begin{cases} \dot{r} = arz, \\ \dot{z} = \mu_2 + br^2 - z^2, \end{cases} \tag{3.12}$$

which is completely integrable. That is, the function

$$F(r, z) = \frac{a}{2} r^{2/a} \left[\mu_2 + \frac{r^2}{1+a} - z^2 \right] \tag{3.13}$$

is constant along solution curves.

We can find that there exists small negative values of μ_1 such that a stable limit cycle exists. The existence of this limit cycle is outlined in detail by Kuznetsov in [10], where it says that as the values of μ_1 and μ_2 approach the curve

$$P = \left\{ (\mu_1, \mu_2) : \mu_1 = \frac{-a}{3a+2}\mu_2 + \mathcal{O}(|\mu_2|^{\frac{3}{2}}), \mu_2 < 0 \right\} \tag{3.14}$$

from the right, the period of the cycle goes to infinity. This kind of bifurcation is referred to as a *cycle blow-up*, but it is also known to be called a *blue sky catastrophe*.

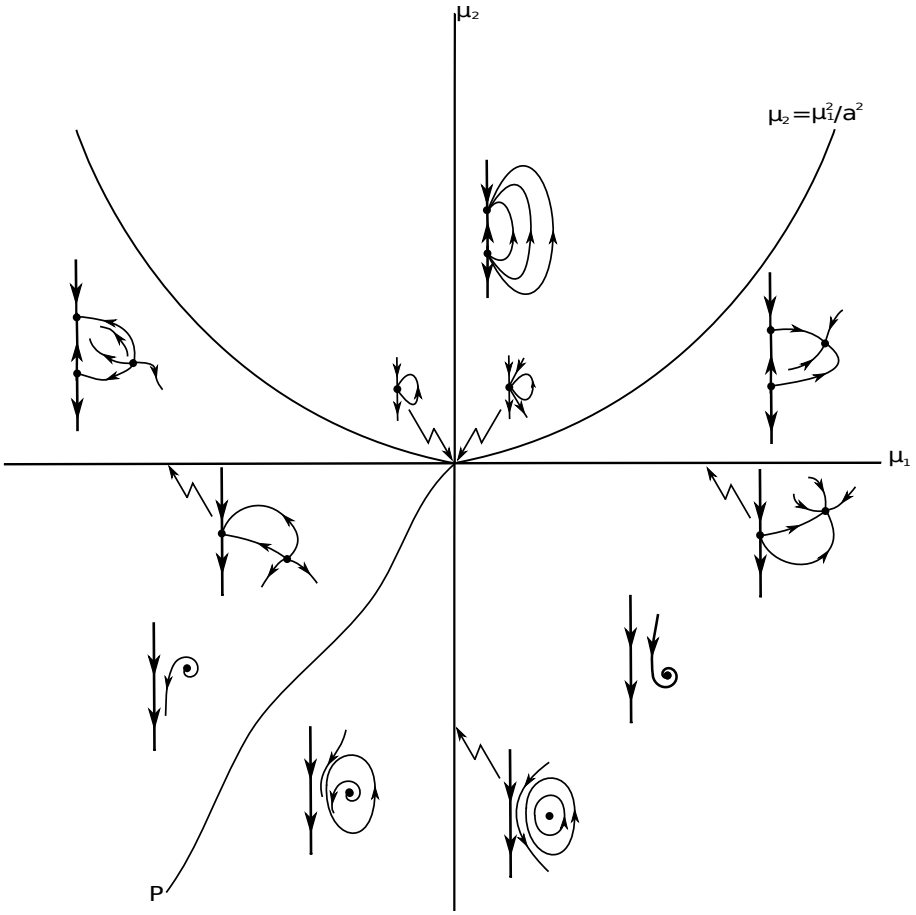

Figure 3.3: The universal unfolding when $b = +1$, $a < 0$. On the curve $\mu_2 = \mu_1^2/a^2$ phase portraits are topologically equivalent to those above the branches of the curve. The phase portrait at the origin is determined by the value of a; the left case being when $a \leq -1$ and the right when $a \in (-1, 0)$.

The analysis of this bifurcation is very complicated and is beyond the scope of this thesis.

We have now completely described the bifurcation diagram of the case when $b = +1$ and $a < 0$. A sketch of the unfolding and corresponding phase portraits is offered in Figure 3.3, where we see that the cases when $a \in [-1, 0)$ and $a < -1$ differ only at the origin. The diagram presented is based on that which is given by Kuznetsov in [10].

We now turn to the case when $b = -1$. When $a < 0$ the unfolding is fairly

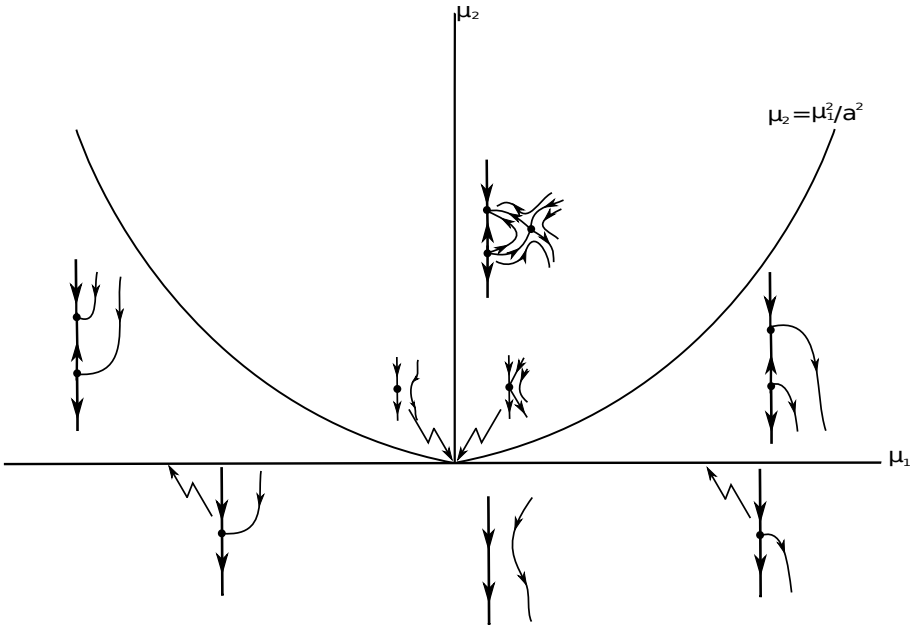

Figure 3.4: The universal unfolding when $b = -1$, $a < 0$. On the curve $\mu_2 = \mu_1^2/a^2$ phase portraits are topologically equivalent to those below the branches of the curve. The phase portrait at the origin is determined by the value of a; the left case being when $a \in [-1, 0)$ and the right when $a < -1$.

straightforward, and the results are comparable to those when $b = +1$ and $a < 0$. We see that the fixed point $(r, z) = (\sqrt{\mu_2 - \mu_1^2/a^2}, -\mu_1/a)$ does not undergo a Hopf bifurcation, but remains a saddle point in the region $\mu_2 > \mu_1^2/a^2$, where it exists. We can perform similar inspections on the fixed points $(0, \pm\sqrt{\mu_2})$ to determine their stability, and arrive at the bifurcation diagram and phase portraits given by Figure 3.4.

The last case, when $b = -1$ and $a > 0$, is vastly different from the previous three cases. The fixed point $(r, z) = (\sqrt{\mu_2 - \mu_1^2/a^2}, -\mu_1/a)$ can now change stability, and therefore a Hopf bifurcation occurs when $\mu_1 = 0$ and $\mu_2 > 0$. As in our earlier work, the system becomes integrable under these assumptions and we have that the function

$$G(r, z) = \frac{a}{2} r^{2/a} \left[\mu_2 - \frac{1}{1+a} r^2 - z^2 \right] \tag{3.15}$$

is constant on the solution curves of the system. This tells us that there exists a

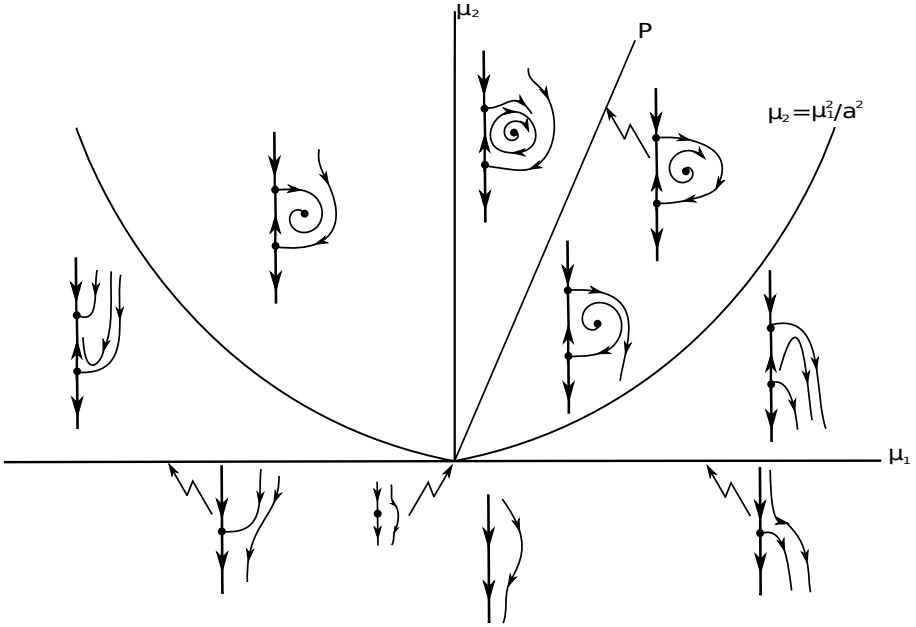

Figure 3.5: The universal unfolding when $b = -1$, $a > 0$. On the curve $\mu_2 = \mu_1^2/a^2$ phase portraits are topologically equivalent to those below the branches of the curve.

stable limit cycle that forms for sufficiently small values of $\mu_1 > 0$. Furthermore, as before we had a cycle blow-up, we now have a pair of fixed points that will draw in the limit cycle in as its period increases. That is, on the curve

$$P = \left\{ (\mu_1, \mu_2) : \mu_1 = \frac{-a}{3a+2}\mu_2 + \mathcal{O}(|\mu_2|^{\frac{3}{2}}), \mu_2 > 0 \right\} \tag{3.16}$$

a heteroclinic orbit can be observed. Again, the proof of this is very difficult and the reader can refer to either [6] or [10] for the results.

We now have all of the required information to create a sufficient bifurcation diagram for the case $b = -1$ and $a > 0$. The unfolding and its corresponding phase portraits are given in Figure 3.5, and we now have a clear picture of the four possible unfoldings for the Zero-Hopf bifurcation.

It is worth noting that the uncoupling with θ is only valid up to finitely many elements of the normal form due to the fact that as we add terms to the normal form the size of the domain of validity of the normal form given in equation (3.2)

decreases to zero. That is, this uncoupling with θ disappears in the neglected higher order terms, and therefore cannot be omitted. However, we note that we only require terms up to the third order to fully determine the nature of each bifurcation that is present in the four cases, and hence for small enough values of r and z we obtain the bifurcation diagrams given in this chapter.

Now that we have analyzed and understood the different possible unfoldings for the Zero-Hopf bifurcation, we are able to apply this theory to our work with delay differential equations. In the coming chapters we will work to reduce the phase space from infinite dimensional to the three dimensional centre manifold and therefore observe the system as it behaves on this manifold. A major difference between the system we have presented in (1.5) to that of Wei and Jiang's [16] is that their system will only allow for the cases when $b = -1$, but we will see that the added delay in velocity will open up the possibilities to all four of the unfoldings presented in this chapter. For that reason, we are able to obtain much more complete dynamics in system (1.5), as well as more detailed results.

Chapter 4

The Centre Manifold Reduction of DDEs

In this chapter, we use the methods outlined by Faria and Magalhães in [4] and [5] for the centre manifold reduction of delay differential equations with parameters. This will allow us to move from an infinite dimensional phase space into the finite dimensional centre manifold where the most interesting dynamics of system (1.5) can be observed. We will apply this method to system (1.5) in order to observe and classify the Zero-Hopf bifurcation that occurs.

To begin, we consider for $\tau \geq 0$, the phase space $C = C([-\tau, 0]; \mathbb{C}^n)$, the space of continuous functions from the interval $[-\tau, 0]$ into $\mathbb{C}^n$. Consider the following retarded functional differential equation with parameters

$$\dot{z}(t) = L(\mu)z_t + G(z_t, \mu) \tag{4.1}$$

where $\mu \in V$, a neighbourhood of zero in $\mathbb{R}^p$, $z_t(\theta) = z(t+\theta)$, $-\tau \leq \theta \leq 0$, $L : C \to \mathbb{C}^n$ is a bounded linear operator and $G : C \times \mathbb{R}^p \to \mathbb{C}^n$ is some sufficiently smooth function such that $G(0, 0) = 0$ and $D_u G(0, 0) = 0$.

By denoting $L_0 = L(0)$ the linear homogeneous retarded functional differential

equation at $\mu = 0$ can be written

$$\dot{z}(t) = L_0 z_t. \tag{4.2}$$

From Reisz's Representation Theorem, L_0 has the form

$$L_0\varphi = \int_{-\tau}^{0} d\eta(\theta)\varphi(\theta), \quad \varphi \in C \tag{4.3}$$

where $\eta(\theta)$, $-\tau \leq \theta \leq 0$, is an $n \times n$ matrix whose elements are of bounded variation. Therefore, equation (4.2) becomes

$$\dot{z}(t) = \int_{-\tau}^{0} d\eta(\theta) z(t+\theta). \tag{4.4}$$

Let $\mathcal{A}_0$ be the infinitesimal generator of the semigroup of solutions (see [7] for details) to equation (4.2), we have $\mathcal{A}_0\varphi = \dot{\varphi}$ with domain

$$D(\mathcal{A}_0) = \left\{ \varphi \in C^1([-\tau, 0], \mathbb{C}^n) : \dot{\varphi}(0) = \int_{-\tau}^{0} d\eta(\theta)\varphi(\theta) \right\}. \tag{4.5}$$

Define $C^* = C([-\tau, 0], \mathbb{C}^{n*})$, where $\mathbb{C}^{n*}$ is the space of row vectors. Then for $\varphi \in C$ and $\psi \in C^*$ we define the bilinear form

$$\langle \psi, \varphi \rangle = \psi(0)\varphi(0) - \int_{-\tau}^{0} \int_{0}^{\theta} \psi(\xi - \theta) d\eta(\theta) \varphi(\xi) d\xi. \tag{4.6}$$

Call Λ the set of eigenvalues of the operator $\mathcal{A}_0$ with zero real part, and let P be the generalized eigenspace associated with the eigenvalues in Λ. Then for the purpose of this paper we can assume without any loss of generality that $\dim P = m$ is finite, and denote P^* as the generalized eigenspace of the adjoint of $\mathcal{A}_0$ in C^*. Now C can be decomposed by Λ such that $C = P \oplus Q$, where

$$Q = \{\varphi \in C : \langle \psi, \varphi \rangle = 0 \text{ for all } \psi \in P^*\}. \tag{4.7}$$

Then there exists bases Φ, Ψ for P, P^* respectively satisfying $\langle \Psi, \Phi \rangle = I$. Using these bases we can now project solutions from the infinite dimensional space C to the finite dimensional centre manifold P.

Then, as described by Faria and Magalhães in [4] and [5], we consider the phase space BC of functions from $[-\tau, 0]$ to $\mathbb{C}^n$ uniformly continuous on $[-\tau, 0)$ and with a jump discontinuity at 0. Therefore any element in BC can be written in the form $\phi = \varphi + X_0 c$, where X_0 is the matrix valued function given by

$$X_0(\theta) = \begin{cases} I, & \theta = 0 \\ 0, & \theta \in [-\tau, 0) \end{cases}, \tag{4.8}$$

$\varphi \in C$, and c is a vector in $\mathbb{C}^n$. This allows us to consider equation (4.1) in BC as the abstract ordinary differential equation

$$\frac{d}{dt}u = \mathcal{A}u + X_0 F(u, \mu) \tag{4.9}$$

where

$$F(\varphi, \mu) = (L(\mu) - L_0)\varphi + G(\varphi, \mu) \tag{4.10}$$

for $\varphi \in C$, $\mu \in V$ and the operator $\mathcal{A} : C^1 \to BC$ is an extension of the infinitesimal generator $\mathcal{A}_0$ and is given by

$$\mathcal{A}\varphi = \dot{\varphi} + X_0[L_0\varphi - \dot{\varphi}(0)]. \tag{4.11}$$

Then $\pi : BC \to P$ is the continuous projection

$$\pi(\varphi + X_0 c) = \Phi[\langle \Psi, \varphi \rangle + \Psi(0)c] \tag{4.12}$$

which allows us to decompose the space BC by Λ such that $BC = P \oplus \text{Ker } \pi$. Since we have that $Q \subsetneq \text{Ker } \pi$ we may rewrite equation (4.9) as

$$\begin{aligned} \dot{x} &= Jx + \Psi(0)F(\Phi x + y, \mu) \\ \frac{d}{dt}y &= \mathcal{A}_{Q^1} y + (I - \pi)X_0 F(\Phi x + y, \mu) \end{aligned} \tag{4.13}$$

where $x \in \mathbb{C}^m$, $y \in Q^1 = Q \cap C^1$, $\mathcal{A}_{Q^1}$ is the operator $\mathcal{A}$ restricted to functions in Q^1, and the $m \times m$ matrix J satisfies the ordinary differential equations $d\Phi/d\theta = \Phi J$ and $d\Psi/d\theta = -J\Psi$.

We may use the Taylor series expansion of F at $(x, y, \mu) = (0, 0, 0)$ to expand the nonlinear terms in equation (4.13) and obtain

$$\begin{aligned} \dot{x} &= Jx + \sum_{j\geq 2} \frac{1}{j!} f_j^1(x, y, \mu) \\ \frac{d}{dt} y &= \mathcal{A}_{Q^1} y + \sum_{j\geq 2} \frac{1}{j!} f_j^2(x, y, \mu) \end{aligned} \tag{4.14}$$

where $f_j^i(x, y, \mu)$ are the homogeneous polynomials of degree j.

The first equation in (4.14) gives us a differential equation on the centre manifold in terms of the unknowns x and y. We now apply the theory outlined in [4] and [5] to obtain a normal form of the equations in (4.14) such that $y = 0$ is a solution to the second equation and therefore we get the normal form on the centre manifold given by

$$\dot{x} = Jx + g_2^1(x, 0, \mu) + g_3^1(x, 0, \mu) + \mathcal{O}(|\mu|^2 + |x||\mu|^2 + |x|^2|\mu| + |x|^3), \tag{4.15}$$

where g_2^1 and g_3^1 are the second and third order terms in (x, μ), respectively.

4.1 Necessary Terms in the Normal Form

In this thesis we consider the case when $\Lambda = \{i\omega, -i\omega, 0\}$, and thus we will use normal form theory to calculate the necessary terms on the centre manifold corresponding to this choice of Λ. It follows that $J = \text{diag}(i\omega, -i\omega, 0)$, m is taken to be 3 from the definition above, and since the Zero-Hopf bifurcation is a codimension 2 bifurcation, p is taken to be 2.

First, let $V_j(\mathbb{C}^3 \times \text{Ker } \pi)$ be the space of homogeneous polynomials of degree j in the variables (x, μ) with coefficients in $\mathbb{C}^3 \times \text{Ker } \pi$. Define $M_j : V_j(\mathbb{C}^3 \times \text{Ker } \pi) \to V_j(\mathbb{C}^3 \times \text{Ker } \pi)$ such that

$$M_j(p, h) = (M_j^1 p, M_j^2 h) \tag{4.16}$$

where

$$M_j^1 p(x,\mu) = D_x p(x,\mu)Jx - Jp(x,\mu) = i\omega \begin{pmatrix} x_1\dfrac{\partial p_1}{\partial x_1} - x_2\dfrac{\partial p_1}{\partial x_2} - p_1 \\ x_1\dfrac{\partial p_2}{\partial x_1} - x_2\dfrac{\partial p_2}{\partial x_2} + p_2 \\ x_1\dfrac{\partial p_3}{\partial x_1} - x_2\dfrac{\partial p_3}{\partial x_2} \end{pmatrix},$$
$$M_j^2 h(x,\mu) = D_x h(x,\mu)Jx - \mathcal{A}_{Q^1} h(x,\mu), \tag{4.17}$$

with $p(x,\mu) \in V_j(\mathbb{C}^3)$ and $h(x,\mu)(\theta) \in V_j(\text{Ker } \pi)$. We now have the decomposition $V_j(\mathbb{C}^3) = \text{Im}(M_j^1) \otimes \text{Ker}(M_j^1)$ for $j \geq 2$.

Introduce the nonlinear change of coordinates

$$\begin{aligned} x &= \hat{x} + U_2^1(\hat{x},\mu) \\ y &= \hat{y} + U_2^2(\hat{x},\mu), \end{aligned} \tag{4.18}$$

where

$$\begin{aligned} U_2^1(x,\mu) &= (M_1^1)^{-1} Proj_{\text{Im}(M_2^1)} f_2^1(x,0,\mu), \\ U_2^2(x,\mu) &= (M_2^2)^{-1} f_2^2(x,0,\mu). \end{aligned} \tag{4.19}$$

Equation (4.14) now becomes

$$\begin{aligned} \dot{x} &= (I + D_x U_2^1(x,\mu))^{-1}\big[Jx + JU_2^1(x,\mu) + \sum_{j\geq 2} f_j^1(x + U_2^1(x,\mu), y + U_2^2(x,\mu))\big] \\ \frac{d}{dt}y &= \mathcal{A}_{Q^1} y + \mathcal{A}_{Q^1} U_2^2(x,\mu) - D_x U_2^2(x,\mu)\dot{x} + \sum_{j\geq 2} f_j^2(x + U_2^1(x,\mu), y + U_2^2(x,\mu)) \end{aligned} \tag{4.20}$$

upon dropping the hats.

For $||x||$ small we have that

$$(I + D_x U_2^1(x,\mu))^{-1} \approx I - D_x U_2^1(x,\mu) + (D_x U_2^1(x,\mu))^2, \tag{4.21}$$

and using Taylor's Theorem we obtain

$$f_2^1(x+U_2^1(x,\mu), y+U_2^2(x,\mu)) = f_2^1(x,y) + D_x f_2^1(x,y)U_2^1(x,\mu) + D_y f_2^1(x,y)U_2^2(x,\mu) + h.o.t.,$$

$$f_3^1(x + U_2^1(x,\mu), y + U_2^2(x,\mu)) = f_3^1(x,y) + h.o.t..$$

Therefore we now have the normal form on the centre manifold given by equation (4.15) where

$$\begin{aligned} g_2^1(x,0,\mu) =& Proj_{Ker(M_2^1)} f_2^1(x,0,\mu) \\ g_3^1(x,0,\mu) =& Proj_{Ker(M_3^1)} \Big[f_3^1(x,0,\mu) + D_x f_2^1(x,0,\mu) U_2^1(x,\mu) + D_y f(x,0,\mu) U_2^2(x,\mu) \\ & - D_x U_2^1(x,\mu) J U_2^1(x,\mu) - D_x U_2^1(x,\mu) f_2^1(x,0,\mu) + (D_x U_2^1(x,\mu))^2 Jx \Big]. \end{aligned} \tag{4.22}$$

Consider the basis $\{\mu^p x^q e_k : k = 1,2,3, p \in \mathbb{N}_0^2, q \in \mathbb{N}_0^3, |p| + |q| = j\}$ of $V_j(\mathbb{C}^3)$, where $e_1 = (1,0,0)^T$, $e_2 = (0,1,0)^T$ and $e_3 = (0,0,1)^T$. Then for $j = 2$, upon finding the images of each basis element under M_2^1, we find that $\mathrm{Ker}(M_2^1)$ is spanned by

$$\mu_1 x_1 e_1, \mu_2 x_1 e_1, x_1 x_3 e_1,$$

$$\mu_1 x_2 e_2, \mu_2 x_2 e_2, x_2 x_3 e_2,$$

$$x_1 x_2 e_3, \mu_1 x_3 e_3, \mu_2 x_3 e_3, \mu_1^2 e_3, \mu_2^2 e_3, \mu_1 \mu_2 e_3, x_3^2 e_3.$$

Similarly, we find that $\mathrm{Ker}(M_3^1)$ is spanned by

$$\mu_1\mu_2 x_1 e_1, \mu_1^2 x_1 e_1, \mu_2^2 x_1 e_1, \mu_1 x_1 x_3 e_1, \mu_2 x_1 x_3 e_1, x_1^2 x_2 e_1, x_1 x_3^2 e_1,$$

$$\mu_1\mu_2 x_2 e_2, \mu_1^2 x_2 e_2, \mu_2^2 x_2 e_2, \mu_1 x_2 x_3 e_2, \mu_2 x_2 x_3 e_2, x_1 x_2^2 e_2, x_2 x_3^2 e_2,$$

$$\mu_1 x_1 x_2 e_3, \mu_2 x_1 x_2 e_3, \mu_1 x_3^2 e_3, \mu_2 x_3^2 e_3, \mu_1\mu_2 x_3 e_3, x_1 x_2 x_3 e_3, x_3^3 e_3.$$

To see where each individual basis element is taken under the operator M_j^1 see [19].

The condition that $y = 0$ must satisfy the second equation in (4.14) comes from the choice of the nonlinear change of coordinates given in (4.19). This guarantees that the range of M_j^2 is the whole space $V_j(\mathrm{Ker}\ \pi)$, and therefore gives higher order terms that all must include some power of y. This solution $y = 0$ is not a trivial result by any respect, and it is proven with a certain degree of difficulty by Faria

and Magalhães in [4] and [5]. This is one of the main results given in their papers and it comes from the application of tradition Normal Form Reduction applied to the ordinary differential equation in the complement space Q. Faria and Magalhães tell us that regardless of the ordinary differential equation that we are given in the compliment space, all terms that do not contain a variable from that compliment space will be eliminated under the proper change of variables to produce the normal form. Thus we have obtained a normal form on a finite dimensional manifold tangent to the subspace P for the linearized equation at $z = 0$ and $\mu = 0$.

Chapter 5

The Reduced System

Here we will apply the theory from the previous chapter to reduce system (1.5) from a delay-differential equation with an infinite dimensional phase space to an ordinary differential equation on the three dimensional centre manifold. This reduction will allow us to analyze the Zero-Hopf bifurcation in the system and help us classify the conditions necessary to induce the different possible results with this type of bifurcation.

To begin, suppose $\varepsilon > 0$ and $\varepsilon^2 - a^2 < 2$. Then if $b = 1$ and $\tau = \tau_0 \neq \varepsilon + a$, Theorem 2.1 tells us that the characteristic equation has a zero root and a simple pair of purely imaginary roots given by $\pm i\omega_0$.

By setting $u_1 = x$, $u_2 = \dot{x}$ we get from (1.5) the following first order delay differential equation,

$$\begin{cases} \dot{u_1} = u_2, \\ \dot{u_2} = -u_1 - \varepsilon(u_1^2 - 1)u_2 + g(u_2(t-\tau), u_1(t-\tau)), \end{cases} \tag{5.1}$$

where the Taylor expansion of g is given by

$$\begin{aligned} g(x,y) =& ay + bx + \frac{1}{2}g_{xx}(0,0)x^2 + g_{xy}(0,0)xy + \frac{1}{2}g_{yy}(0,0)y^2 + \frac{1}{3!}g_{xxx}(0,0)x^3 \\ &+ \frac{1}{2}g_{xxy}(0,0)x^2y + \frac{1}{2}g_{yyx}(0,0)xy^2 + \frac{1}{3!}g_{yyy}(0,0)y^3 + \mathcal{O}(|x,y|^4). \end{aligned} \tag{5.2}$$

After the scaling $t \to t/\tau$, system (5.1) becomes

$$\begin{cases} \dot{u_1} = \tau u_2, \\ \dot{u_2} = -\tau u_1 - \varepsilon\tau(u_1^2 - 1)u_2 + \tau\Big[au_2(t-1) + bu_1(t-1) + \frac{1}{2}g_{u_1u_1}(0,0)u_1^2(t-1) \\ \quad + g_{u_1u_2}(0,0)u_1(t-1)u_2(t-1) + \frac{1}{2}g_{u_2u_2}(0,0)u_2^2(t-1) + \frac{1}{6}g_{u_1u_1u_1}(0,0)u_1^3(t-1) \\ \quad + \frac{1}{2}g_{u_1u_1u_2}(0,0)u_1^2(t-1)u_2(t-1) + \frac{1}{2}g_{u_2u_2u_1}(0,0)u_1(t-1)u_2^2(t-1) \\ \quad + \frac{1}{6}g_{u_2u_2u_2}(0,0)u_2^3(t-1)\Big] + \mathcal{O}(|u_1,u_2|^4). \end{cases} \tag{5.3}$$

If we let $\mu_1 = b - 1$ and $\mu_2 = \tau - \tau_0$, then μ_1 and μ_2 become bifurcation parameters and system (5.3) now becomes

$$\begin{cases} \dot{u_1} = \tau_0 u_2 + \mu_2 u_2, \\ \dot{u_2} = -\tau_0 u_1 + \tau_0 u_1(t-1) + \tau_0 a u_2(t-1) + \varepsilon\tau_0 u_2 - \mu_2 u_1 \\ \quad + \varepsilon\mu_2 u_2 + a\mu_2 u_2(t-1) + \tau_0\mu_1 u_1(t-1) + \mu_2 u_1(t-1) - \varepsilon\tau_0 u_1^2 u_2 - \varepsilon\mu_2 u_1^2 u_2 \\ \quad + \mu_1\mu_2 u_1(t-1) + \frac{1}{2}\tau_0 g_{u_1u_1}(0,0)u_1^2(t-1) + \tau_0 g_{u_1u_2}(0,0)u_1(t-1)u_2(t-\tau) \\ \quad + \frac{1}{2}\tau_0 g_{u_2u_2}(0,0)u_2^2(t-1) + \frac{1}{2}g_{u_1u_1}(0,0)\mu_2 u_1^2(t-1) \\ \quad + g_{u_1u_2}(0,0)\mu_2 u_1(t-1)u_2(t-1) + \frac{1}{2}g_{u_2u_2}(0,0)\mu_2 u_2^2(t-1) \\ \quad + \frac{1}{6}\tau_0 g_{u_1u_1u_1}(0,0)u_1^3(t-1) + \frac{1}{2}\tau_0 g_{u_1u_1u_2}(0,0)u_1^2(t-1)u_2(t-1) \\ \quad + \frac{1}{2}\tau_0 g_{u_2u_2u_1}(0,0)u_1(t-1)u_2^2(t-1) + \frac{1}{6}\tau_0 g_{u_2u_2u_2}(0,0)u_2^3(t-1) + h.o.t., \end{cases} \tag{5.4}$$

where $h.o.t.$ stands for "higher order terms" and in this case represents the terms of order four and more in u_1, u_2, μ_1 and μ_2.

Linearizing (5.4) around $(u_1, u_2, \mu_1, \mu_2) = (0,0,0,0)$ we get

$$\begin{cases} \dot{u_1} = \tau_0 u_2, \\ \dot{u_2} = -\tau_0 u_1 + \varepsilon\tau_0 u_2 + \tau_0 u_1(t-1) + \tau_0 a u_2(t-1). \end{cases} \tag{5.5}$$

By letting

$$\eta(\theta) = \mathbb{A}\delta(\theta) + \mathbb{B}\delta(\theta + 1) \tag{5.6}$$

such that

$$\mathbb{A} = \begin{pmatrix} 0 & \tau_0 \\ -\tau_0 & \varepsilon\tau_0 \end{pmatrix}, \qquad \mathbb{B} = \begin{pmatrix} 0 & 0 \\ \tau_0 & a\tau_0 \end{pmatrix}, \tag{5.7}$$

we can define the operator

$$L\varphi = \int_{-1}^{0} d\eta(\theta)\varphi(\theta), \quad \forall \varphi \in C = C([-1,0],\mathbb{C}^2). \tag{5.8}$$

Define $X = (u_1, u_2)^T$. Then (5.4) can be rewritten in the following form,

$$\dot{X}(t) = LX_t + F(X_t, \mu), \tag{5.9}$$

where $F(X_t,\mu) = (F^1, F^2)^T$ is given by

$$\begin{aligned} F^1 &= \mu_2 u_2, \\ F^2 =& \mu_2 u_1 + \varepsilon\mu_2 u_2 + a\mu_2 u_2(t-1) + \tau_0\mu_1 u_1(t-1) + \mu_2 u_1(t-1) \\ &- \varepsilon\tau_0 u_1^2 u_2 - \varepsilon\mu_2 u_1^2 u_2 + \mu_1\mu_2 u_1(t-1) + \frac{1}{2}\tau_0 g_{u_1u_1}(0,0)u_1^2(t-1) \\ &+ \tau_0 g_{u_1u_2}(0,0)u_1(t-1)u_2(t-1) + \frac{1}{2}\tau_0 g_{u_2u_2}(0,0)u_2^2(t-1) + \\ &\frac{1}{2}g_{u_1u_1}(0,0)\mu_2 u_1^2(t-1) + g_{u_1u_2}(0,0)\mu_2 u_1(t-1)u_2(t-1) + \frac{1}{2}g_{u_2u_2}(0,0)\mu_2 u_2^2(t-1) \\ &+ \frac{1}{6}\tau_0 g_{u_1u_1u_1}(0,0)u_1^3(t-1) + \frac{1}{2}\tau_0 g_{u_1u_1u_2}(0,0)u_1^2(t-1)u_2(t-1) \\ &+ \frac{1}{2}\tau_0 g_{u_2u_2u_1}(0,0)u_1(t-1)u_2^2(t-1) + \frac{1}{6}\tau_0 g_{u_2u_2u_2}(0,0)u_2^3(t-1) + h.o.t. \end{aligned} \tag{5.10}$$

Using the definition of η above we can simplify the bilinear form in (4.6) to get

$$\langle \psi, \varphi \rangle = \psi(0)\varphi(0) + \int_{-1}^{0} \psi(\xi+1)\mathbb{B}\varphi(\xi)d\xi. \tag{5.11}$$

The infinitesimal generator $\mathcal{A} : C^1([-1,0],\mathbb{C}^2) \to BC$ is defined as

$$\mathcal{A}\varphi(\theta) = \dot{\varphi} + X_0[L\varphi - \dot{\varphi}(0)] = \begin{cases} \dot{\varphi} & \text{if } -1 \le \theta < 0, \\ \displaystyle\int_{-1}^{0} d\eta(t)\varphi(t), & \text{if } \theta = 0, \end{cases} \tag{5.12}$$

with adjoint $\mathcal{A}^* : C^1([0,1],\mathbb{C}^{2*}) \to BC$ given by

$$\mathcal{A}^*\psi(s) = -\dot{\psi} + X_0[L^*\psi + \dot{\psi}(0)] = \begin{cases} \dot{\psi} & \text{if } 0 \le s < 1, \\ \displaystyle\int_{0}^{1} \psi(-t)d\eta(t), & \text{if } s = 0. \end{cases} \tag{5.13}$$

Then $\mathcal{A}$ and $\mathcal{A}^*$ have eigenvalues $0, i\omega_0\tau_0$ and $-i\omega_0\tau_0$ for which we must now compute their respective eigenvectors.

Lemma 5.1. *There exists bases* $\Phi = (\varphi_1, \bar{\varphi}_1, \varphi_2)$ *and* $\Psi = (\bar{\psi}_1, \psi_1, \psi_2)^T$ *of the centre space* P *and its adjoint* P^* *such that* $\dot{\Phi} = \Phi J$, $\dot{\Psi} = J\Psi$ *and* $\langle \Psi, \Phi \rangle = I$, *where*

$$\begin{aligned}
&\varphi_1(\theta) = (1, i\omega_0)^T e^{i\omega_0\tau_0\theta}, \qquad \varphi_2(\theta) = (1,0)^T \\
&\psi_1(s) = D(1,\sigma)e^{i\omega_0\tau_0 s}, \qquad \psi_2(s) = D_1(\varepsilon + a, -1) \\
&J = diag(i\omega_0\tau_0, -i\omega_0\tau_0, 0), \qquad \sigma = \frac{i\omega_0}{1 - e^{i\omega_0\tau_0}}, \\
&D = \frac{1}{1 - i\sigma\omega_0 + \tau_0\sigma e^{i\omega_0\tau_0}(1 - ia\omega_0)}, \qquad D_1 = \frac{1}{\varepsilon + a - \tau_0}.
\end{aligned}$$

Proof: Suppose $\varphi_1(\theta) = (1, \rho)^T e^{i\omega_0\tau_0\theta}$ is an eigenvector of $\mathcal{A}$ corresponding to $i\omega_0\tau_0$. Then $\mathcal{A}\varphi_1(\theta) = i\omega_0\tau_0\varphi_1(\theta)$. From the definition of $\mathcal{A}$ we get

$$\mathbb{A}\varphi_1(0) + \mathbb{B}\varphi_1(-1) = i\omega_0\tau_0\varphi_1(0)$$

which gives us that

$$\tau_0 \begin{pmatrix} -i\omega_0 & 1 \\ -1 + e^{-i\omega_0\tau_0} & \varepsilon - ae^{-i\omega_0\tau_0} - i\omega_0 \end{pmatrix} \begin{pmatrix} 1 \\ \rho \end{pmatrix} = \begin{pmatrix} 0 \\ 0 \end{pmatrix},$$

which gives $\rho = i\omega_0$. Similarly suppose $\varphi_2(\theta)$ is the eigenvector of $\mathcal{A}$ corresponding to 0. From the definition of $\mathcal{A}$, we have that $\varphi_2(\theta)$ is a constant vector $(\alpha, \beta)^T$ such that

$$(\mathbb{A} + \mathbb{B}) \begin{pmatrix} \alpha \\ \beta \end{pmatrix} = 0$$

from which we obtain $\varphi_2(\theta) = (1,0)^T$. Let $\Phi = (\varphi_1(\theta), \bar{\varphi}_1(\theta), \varphi_2(\theta))$. Then it is easy to check that $\dot{\Phi} = \Phi J$.

Now suppose $\psi_1(s) = D(1,\sigma)e^{i\omega_0\tau_0 s}$ is an eigenvector of $\mathcal{A}^*$ corresponding to $-i\omega_0\tau_0$. Then $\mathcal{A}^*\psi_1(s) = -i\omega_0\tau_0\psi_1(s)$. Then from the definition of $\mathcal{A}^*$ we have

$$\psi_1(0)\mathbb{A} + \psi_1(1)\mathbb{B} = -i\omega_0\tau_0\psi_1(0)$$

or equivalently

$$\tau_0 \begin{pmatrix} 1, & \sigma \end{pmatrix} \begin{pmatrix} i\omega_0 & 1 \\ -1 + e^{i\omega_0\tau_0} & \varepsilon + ae^{i\omega_0\tau_0} + i\omega_0 \end{pmatrix} = (0,0)$$

which gives us

$$\sigma = \frac{i\omega_0}{1 - e^{i\omega_0\tau_0}}.$$

Suppose that $\psi_2(s)$ is the eigenvector of $\mathcal{A}^*$ corresponding to 0. From the definition of $\mathcal{A}^*$, we have that $\psi_2(s)$ is a constant vector (α,β) such that

$$(\alpha,\beta)(\mathbb{A} + \mathbb{B}) = 0$$

which gives $\psi_2(s) = D_1(\varepsilon + a, -1)$. Let $\Psi = (\bar{\psi_1}(s), \psi_1(s), \psi_2(s))$. Then we have $\dot{\Psi} = -J\Psi$.

It can be checked that $\langle \psi_1, \varphi_1 \rangle = 0$, $\langle \psi_2, \varphi_1 \rangle = 0$ and $\langle \psi_1, \varphi_2 \rangle = 0$. In order to assure $\langle \bar{\psi_1}, \varphi_1 \rangle = 1$, $\langle \psi_2, \varphi_2 \rangle = 1$, we must determine the factors D, D_1. Since

$$\begin{aligned}
\langle \bar{\psi}_1, \varphi_1 \rangle &= \bar{D}\Big[(1,\bar{\sigma})\begin{pmatrix}1\\ i\omega_0\end{pmatrix} + \int_{-1}^{0}(1,\bar{\sigma})e^{-i\omega_0\tau_0(\xi+1)}\mathbb{B}\begin{pmatrix}1\\ i\omega_0\end{pmatrix}e^{i\omega_0\tau_0\xi}d\xi\Big],\\
&= \bar{D}\big[1 + i\bar{\sigma}\omega_0 + \tau_0\bar{\sigma}e^{-i\omega_0\tau_0}(1+ia\omega_0)\big]\\
\langle \psi_2, \varphi_2 \rangle &= D_1\Big[(\varepsilon+a,-1)\begin{pmatrix}1\\ 0\end{pmatrix} + \int_{-1}^{0}(\varepsilon+a,-1)\mathbb{B}\begin{pmatrix}1\\ 0\end{pmatrix}d\xi\Big]\\
&= D_1\big[\varepsilon + a - \tau_0\big],
\end{aligned}$$

we get the desired results, finishing the proof of the lemma. ∎

Now let $u = \Phi x + y$ where $x \in \mathbb{C}^3$ and $y \in Q^1 = \{\varphi \in Q : \dot{\varphi} \in C\}$, then we write u as

$$\begin{aligned}
u_1(\theta) &= e^{i\omega_0\tau_0\theta}x_1 + e^{-i\omega_0\tau_0\theta}x_2 + x_3 + y_1(\theta)\\
u_2(\theta) &= i\omega_0 e^{i\omega_0\tau_0\theta}x_1 - i\omega_0 e^{-i\omega_0\tau_0\theta}x_2 + y_2(\theta).
\end{aligned} \tag{5.14}$$

Let

$$\Psi(0) = \begin{pmatrix}\psi_{11} & \psi_{12}\\ \psi_{21} & \psi_{22}\\ \psi_{31} & \psi_{32}\end{pmatrix} = \begin{pmatrix}\bar{D} & \bar{D}\bar{\sigma}\\ D & D\sigma\\ D_1(\varepsilon+a) & -D_1\end{pmatrix}. \tag{5.15}$$

Then System (5.4) is decomposed as

$$\begin{cases}\dot{x} = Jx + \Psi(0)F(\Phi x + y, \mu)\\ \dot{y} = A_{Q^1}y + (I-\pi)X_0F(\Phi x + y, \mu)\end{cases} \tag{5.16}$$

and upon using Taylor's Theorem we obtain

$$\begin{cases}\dot{x} = Jx + f_2^1(x,y,\mu) + f_3^1(x,y,\mu) + h.o.t.,\\ \dot{y} = A_{Q^1}y + f_2^2(x,y,\mu) + f_3^2(x,y,\mu) + h.o.t.,\end{cases} \tag{5.17}$$

where

$$\begin{aligned}
f_2^1(x,y,\mu) &= \begin{pmatrix} \psi_{11}F_2^1(\Phi x+y,\mu)+\psi_{12}F_2^2(\Phi x+y,\mu) \\ \psi_{21}F_2^1(\Phi x+y,\mu)+\psi_{22}F_2^2(\Phi x+y,\mu) \\ \psi_{31}F_2^1(\Phi x+y,\mu)+\psi_{32}F_2^2(\Phi x+y,\mu) \end{pmatrix}, \\
f_2^2(x,y,\mu) &= (I-\pi)X_0 \begin{pmatrix} F_2^1(\Phi x+y,\mu) \\ F_2^2(\Phi x+y,\mu) \end{pmatrix}, \\
f_3^1(x,y,\mu) &= \begin{pmatrix} \psi_{11}F_3^1(\Phi x+y,\mu)+\psi_{12}F_3^2(\Phi x+y,\mu) \\ \psi_{21}F_3^1(\Phi x+y,\mu)+\psi_{22}F_3^2(\Phi x+y,\mu) \\ \psi_{31}F_3^1(\Phi x+y,\mu)+\psi_{32}F_3^2(\Phi x+y,\mu) \end{pmatrix}, \\
f_3^2(x,y,\mu) &= (I-\pi)X_0 \begin{pmatrix} F_3^1(\Phi x+y,\mu) \\ F_3^2(\Phi x+y,\mu) \end{pmatrix}.
\end{aligned} \tag{5.18}$$

Then we are able to compute the normal form of system (5.17) taking the form

$$\dot{x} = Jx + g_2^1(x,0,\mu) + g_3^1(x,0,\mu) + h.o.t. \tag{5.19}$$

First we compute $g_2^1(x,0,\mu)$. From the work in the previous chapter we have that

$$\begin{aligned}
g_2^1(x,0,\mu) &= Proj_{\mathrm{Ker}(M_2^1)} f_2^1(x,0,\mu) + \mathcal{O}(|\mu|^2) \\
&= \begin{pmatrix} (a_{11}\mu_1+a_{12}\mu_2)x_1 + a_{13}x_1x_3 \\ (\bar{a}_{11}\mu_1+\bar{a}_{12}\mu_2)x_2 + \bar{a}_{13}x_2x_3 \\ (a_{21}\mu_1+a_{22}\mu_2)x_3 + a_{23}x_1x_2 + a_{24}x_3^2 \end{pmatrix} + \mathcal{O}(|\mu|^2).
\end{aligned} \tag{5.20}$$

Now expanding out the terms in (5.18) we get

$$
\begin{aligned}
F_2^1 =&\mu_2(i\omega_0 x_1 - i\omega_0 x_2 + y_2(0)), \qquad F_3^1 = 0,\\
F_2^2 =& -\mu_2(x_1 + x_2 + x_3 + y_1(0)) + \varepsilon\mu_2(i\omega_0 x_1 - i\omega_0 x_2 + y_2(0)) + a\mu_2(i\omega_0 e^{-i\omega_0\tau_0}x_1\\
&- i\omega_0 e^{i\omega_0\tau_0}x_2 + y_2(-1)) + \tau_0\mu_1(e^{-i\omega_0\tau_0}x_1 + e^{i\omega_0\tau_0}x_2 + x_3 + y_1(-1)) + \mu_2(e^{-i\omega_0\tau_0}x_1\\
&+ e^{i\omega_0\tau_0}x_2 + x_3 + y_1(-1)) + \frac{1}{2}\tau_0 g_{u_1u_1}(0,0)(e^{-i\omega_0\tau_0}x_1 + e^{i\omega_0\tau_0}x_2 + x_3 + y_1(-1))^2\\
&+ \tau_0 g_{u_1u_2}(0,0)(e^{-i\omega_0\tau_0}x_1 + e^{i\omega_0\tau_0}x_2 + x_3 + y_1(-1))(i\omega_0 e^{-i\omega_0\tau_0}x_1 - i\omega_0 e^{i\omega_0\tau_0}x_2\\
&+ y_2(-1)) + \frac{1}{2}\tau_0 g_{u_2u_2}(0,0)(i\omega_0 e^{-i\omega_0\tau_0}x_1 - i\omega_0 e^{i\omega_0\tau_0}x_2 + y_2(-1))^2,\\
F_3^2 =& -\varepsilon\tau_0(x_1 + x_2 + x_3 + y_1(0))^2(i\omega_0 x_1 - i\omega_0 x_2 + y_2(0)) + \frac{1}{2}g_{u_1u_1}(0,0)\mu_2(e^{-i\omega_0\tau_0}x_1\\
&+ e^{i\omega_0\tau_0}x_2 + x_3 + y_1(-1))^2 + g_{u_1u_2}(0,0)\mu_2(e^{-i\omega_0\tau_0}x_1 + e^{i\omega_0\tau_0}x_2 + x_3 + y_1(-1))\\
&(i\omega_0 e^{-i\omega_0\tau_0}x_1 - i\omega_0 e^{i\omega_0\tau_0}x_2 + y_2(-1)) + \frac{1}{2}g_{u_2u_2}(0,0)\mu_2(i\omega_0 e^{-i\omega_0\tau_0}x_1 - i\omega_0 e^{i\omega_0\tau_0}x_2\\
&+ y_2(-1)) + \frac{1}{6}\tau_0 g_{u_1u_1u_1}(0,0)(e^{-i\omega_0\tau_0}x_1 + e^{i\omega_0\tau_0}x_2 + x_3 + y_1(-1))^3 + \frac{1}{2}\tau_0 g_{u_1u_1u_2}(0,0)\\
&(e^{-i\omega_0\tau_0}x_1 + e^{i\omega_0\tau_0}x_2 + x_3 + y_1(-1))^2(i\omega_0 e^{-i\omega_0\tau_0}x_1 - i\omega_0 e^{i\omega_0\tau_0}x_2 + y_2(-1))\\
&+ \frac{1}{2}\tau_0 g_{u_2u_2u_1}(0,0)(e^{-i\omega_0\tau_0}x_1 + e^{i\omega_0\tau_0}x_2 + x_3 + y_1(-1))(i\omega_0 e^{-i\omega_0\tau_0}x_1 - i\omega_0 e^{i\omega_0\tau_0}x_2\\
&+ y_2(-1))^2 + \frac{1}{6}\tau_0 g_{u_2u_2u_2}(0,0)(i\omega_0 e^{-i\omega_0\tau_0}x_1 - i\omega_0 e^{i\omega_0\tau_0}x_2 + y_2(-1))^3.
\end{aligned}
\tag{5.21}
$$

Therefore, recalling that the characteristic equation gives us $(1+ia\omega_0)e^{-i\omega_0\tau_0} = -\omega_0^2 - i\varepsilon\omega_0 + 1$, we compute the coefficients in (5.20) to be

$$
\begin{aligned}
&a_{11} = \tau_0\bar{D}\bar{\sigma}e^{-i\omega_0\tau_0}, \quad a_{12} = \bar{D}(i\omega_0 - \bar{\sigma}\omega_0^2),\\
&a_{13} = \tau_0\bar{D}\bar{\sigma}(g_{u_1u_1}(0,0)e^{-i\omega_0\tau_0} + i\omega_0 g_{u_1u_2}(0,0)e^{-i\omega_0\tau_0}), \quad a_{21} = \frac{\tau_0}{\tau_0 - \varepsilon - a},\\
&a_{22} = 0, \quad a_{23} = a_{21}(g_{u_1u_1}(0,0) + \omega_0^2 g_{u_2u_2}(0,0)), \quad a_{24} = \frac{1}{2}a_{21}g_{u_1u_1}(0,0).
\end{aligned}
\tag{5.22}
$$

Now to compute $g_3^1(x,0,0)$, recall that

$$\begin{aligned} g_3^1(x,0,\mu) = Proj_{Ker(M_3^1)}\Big[& f_3^1(x,0,\mu) + D_x f_2^1(x,0,\mu)U_2^1(x,\mu) + D_y f(x,0,\mu)U_2^2(x,\mu) \\ & - D_x U_2^1(x,\mu)JU_2^1(x,\mu) - D_x U_2^1(x,\mu)f_2^1(x,0,\mu) + (D_x U_2^1(x,\mu))^2 Jx\Big] \\ = & Proj_{\mathrm{Ker}(M_3^1)} f_3^1(x,0,0) + Proj_{\mathrm{Ker}(M_3^1)} D_x f_2^1(x,0,\mu)U_2^1(x,0) \\ & + Proj_{\mathrm{Ker}(M_3^1)} D_y f(x,0,\mu)U_2^2(x,0) - Proj_{\mathrm{Ker}(M_3^1)} D_x U_2^1(x,\mu)JU_2^1(x,\mu) \\ & - Proj_{\mathrm{Ker}(M_3^1)} D_x U_2^1(x,\mu)f_2^1(x,0,0) + Proj_{\mathrm{Ker}(M_3^1)}(D_x U_2^1(x,0))^2 Jx \\ & + \mathcal{O}(|x||\mu|^2 + |x|^2|\mu|). \end{aligned} \tag{5.23}$$

(i) First we compute $Proj_{\mathrm{Ker}(M_3^1)} f_3^1(x,0,0)$. Since

$$f_3^1(x,0,0) = \tau_0 \begin{pmatrix} \bar{D}\bar{\sigma}H_1(x_1,x_2,x_3) \\ D\sigma H_1(x_1,x_2,x_3) \\ -D_1 H_1(x_1,x_2,x_3) \end{pmatrix}, \tag{5.24}$$

where

$$\begin{aligned} H_1(x_1,x_2,x_3) = & -i\varepsilon\omega_0(x_1-x_2)(x_1+x_2+x_3)^2 + \frac{1}{6}g_{u_1u_1u_1}(0,0)(e^{-i\omega_0\tau_0}x_1 \\ & + e^{i\omega_0\tau_0}x_2 + x_3)^3 + \frac{1}{2}g_{u_1u_1u_2}(0,0)(e^{-i\omega_0\tau_0}x_1 + e^{i\omega_0\tau_0}x_2 + x_3)^2 \\ & (i\omega_0 e^{-i\omega_0\tau_0}x_1 - i\omega_0 e^{i\omega_0\tau_0}x_2) + \frac{1}{2}g_{u_2u_2u_1}(0,0)(e^{-i\omega_0\tau_0}x_1 + e^{i\omega_0\tau_0}x_2 \\ & + x_3)(i\omega_0 e^{-i\omega_0\tau_0}x_1 - i\omega_0 e^{i\omega_0\tau_0}x_2)^2 - \frac{i\omega_0}{6}(e^{-i\omega_0\tau_0}x_1 - e^{i\omega_0\tau_0}), \end{aligned} \tag{5.25}$$

this gives us that

$$Proj_{\mathrm{Ker}(M_2^1)} f_3^1(x,0,0) = \begin{pmatrix} b_{11}x_1^2x_2 + b_{12}x_1x_3^2 \\ \bar{b}_{11}x_1x_2^2 + \bar{b}_{12}x_2x_3^2 \\ b_{21}x_1x_2x_3 + b_{22}x_3^3 \end{pmatrix}, \tag{5.26}$$

such that

$$\begin{aligned}
b_{11} =&\tau_0\bar{D}\bar{\sigma}e^{-i\omega_0\tau_0}\bigg[-2i\varepsilon\omega_0e^{i\omega_0\tau_0}+\frac{1}{3}g_{u_1u_1u_1}(0,0)+\frac{1}{2}g_{u_1u_1u_2}(0,0)(2\omega_0^2-i\omega_0)\\
&+\frac{1}{2}g_{u_2u_2u_1}(0,0)(2\omega_0^2+i\omega_0)-\frac{i\omega_0^3}{3}g_{u_2u_2u_2}(0,0)\bigg],\\
b_{12} =&\tau_0\bar{D}\bar{\sigma}e^{-i\omega_0\tau_0}\bigg[-i\varepsilon\omega_0e^{i\omega_0\tau_0}+\frac{1}{3}g_{u_1u_1u_1}(0,0)+\frac{i\omega_0}{2}g_{u_1u_1u_2}(0,0)\bigg],\\
b_{21} =&-\tau_0D_1\bigg[g_{u_1u_1u_1}(0,0)+\frac{2\omega_0^2}{3}g_{u_2u_2u_1}(0,0)\bigg],\qquad b_{22}=\frac{-\tau_0}{6}D_1g_{u_1u_1u_1}(0,0).
\end{aligned}\tag{5.27}$$

(ii) To compute $Proj_{\mathrm{Ker}(M_3^1)}D_xf_2^1(x,0,\mu)U_2^1(x,0)$ we use

$$\begin{aligned}
U_2^1(x,0)=U_2^1(x,\mu)|_{\mu=0}&=(M_2^1)^{-1}Proj_{Im(M_2^1)}f_2^1(x,0,0)\\
&=\frac{\tau_0}{i\omega_0}\begin{pmatrix}
\bar{D}\bar{\sigma}\Big[g_{u_1u_1}(0,0)(e^{-2i\omega_0\tau_0}x_1^2-2x_1x_2-\frac{1}{3}e^{2i\omega_0\tau_0}x_2^2-x_3^2-e^{i\omega_0\tau_0}x_2x_3)\\
+g_{u_2u_2}(0,0)(-\omega_0^2e^{-2i\omega_0\tau_0}x_1^2-2\omega_0^2x_1x_2+\frac{1}{3}\omega_0^2e^{2i\omega_0\tau_0}x_2^2)\\
+2g_{u_1u_2}(0,0)(i\omega_0e^{-2i\omega_0\tau_0}x_1^2+\frac{1}{3}i\omega_0e^{2i\omega_0\tau_0}x_2^2+\frac{1}{2}i\omega_0e^{i\omega_0\tau_0}x_2x_3)\Big]\\
D\sigma\Big[g_{u_1u_1}(0,0)(\frac{1}{3}e^{-2i\omega_0\tau_0}x_1^2+2x_1x_2-e^{2i\omega_0\tau_0}x_2^2+x_3^2+e^{-i\omega_0\tau_0}x_1x_3)\\
+g_{u_2u_2}(0,0)(-\frac{1}{3}\omega_0^2e^{-2i\omega_0\tau_0}x_1^2+2\omega_0^2x_1x_2+\omega_0^2e^{2i\omega_0\tau_0}x_2^2)\\
+2g_{u_1u_2}(0,0)(\frac{1}{3}i\omega_0e^{-2i\omega_0\tau_0}x_1^2-i\omega_0e^{2i\omega_0\tau_0}x_2^2+\frac{1}{2}i\omega_0e^{-i\omega_0\tau_0}x_1x_3)\Big]\\
-D_1\Big[g_{u_1u_1}(0,0)(\frac{1}{2}e^{-2i\omega_0\tau_0}x_1^2-\frac{1}{2}e^{2i\omega_0\tau_0}x_2^2+2e^{-i\omega_0\tau_0}x_1x_3-2e^{i\omega_0\tau_0}x_2x_3)\\
+g_{u_2u_2}(0,0)(-\frac{1}{2}\omega_0^2e^{-2i\omega_0\tau_0}x_1^2+\frac{1}{2}\omega_0^2e^{2i\omega_0\tau_0}x_2^2)\\
+2g_{u_1u_2}(0,0)(\frac{1}{2}i\omega_0e^{-2i\omega_0\tau_0}x_1^2+\frac{1}{2}i\omega_0e^{2i\omega_0\tau_0}x_2^2+i\omega_0e^{-i\omega_0\tau_0}x_1x_3+i\omega_0e^{i\omega_0\tau_0}x_2x_3)\Big]
\end{pmatrix}.
\end{aligned}\tag{5.28}$$

This gives us

$$Proj_{\mathrm{Ker}(M_3^1)}D_xf_2^1(x,0,0)U_2^1(x,0)=\begin{pmatrix}c_{11}x_1^2x_2+c_{12}x_1x_3^2\\ \bar{c}_{11}x_1x_2^2+\bar{c}_{12}x_2x_3^2\\ c_{21}x_1x_2x_3+c_{22}x_3^3\end{pmatrix},\tag{5.29}$$

where

$$
\begin{aligned}
c_{11} &= \frac{-\tau_0^2\bar{D}\bar{\sigma}}{3i\omega_0}\Big[6\bar{D}\bar{\sigma}e^{-2i\omega_0\tau_0}\Big((g_{u_1u_1}(0,0))^2-\omega_0^4(g_{u_2u_2}(0,0))^2+2i\omega_0^3g_{u_1u_2}(0,0)g_{u_2u_2}(0,0)\\
&\quad+2i\omega_0g_{u_1u_1}(0,0)g_{u_1u_2}(0,0)\Big)+2D\sigma\Big(-7(g_{u_1u_1}(0,0))^2-10\omega_0^2g_{u_1u_1}(0,0)g_{u_2u_2}(0,0)\\
&\quad-4\omega_0^2(g_{u_1u_2}(0,0))^2-7\omega_0^2(g_{u_2u_2}(0,0))^2\Big)+3D_1e^{-i\omega_0\tau_0}\Big((g_{u_1u_1}(0,0))^2\\
&\quad+i\omega_0g_{u_1u_1}(0,0)g_{u_1u_2}(0,0)+i\omega_0^3g_{u_1u_2}(0,0)g_{u_2u_2}(0,0)-\omega_0^2g_{u_1u_1}(0,0)g_{u_2u_2}(0,0)\\
&\quad+2\omega_0^2(g_{u_1u_2}(0,0))^2\Big)\Big],\\
c_{12} &= \frac{-2\tau_0\bar{D}\bar{\sigma}}{i\omega_0}\Big[\bar{D}\bar{\sigma}e^{-2i\omega_0\tau_0}\Big((g_{u_1u_1}(0,0))^2+2i\omega_0g_{u_1u_1}(0,0)g_{u_1u_2}(0,0)\\
&\quad-\omega_0^2g_{u_1u_1}(0,0)g_{u_2u_2}(0,0)\Big)+D\sigma\Big(-2(g_{u_1u_1}(0,0))^2-\omega_0^2g_{u_1u_1}(0,0)g_{u_2u_2}(0,0)\\
&\quad-\omega_0^2(g_{u_1u_2}(0,0))^2\Big)+D_1e^{-i\omega_0\tau_0}\Big((g_{u_1u_1}(0,0))^2+2i\omega_0g_{u_1u_1}(0,0)g_{u_1u_2}(0,0)\Big)\Big],\\
c_{21} &= \frac{2\tau_0^2D_1}{i\omega_0}\Big[\bar{D}\bar{\sigma}e^{-i\omega_0\tau_0}\Big(3(g_{u_1u_1}(0,0))^2+3i\omega_0g_{u_1u_1}(0,0)g_{u_1u_2}(0,0)\\
&\quad+2\omega_0^2(g_{u_1u_2}(0,0))^2+\omega_0^2g_{u_1u_1}(0,0)g_{u_2u_2}(0,0)+3i\omega_0^3g_{u_1u_2}(0,0)g_{u_2u_2}(0,0)\Big)\\
&\quad+D\sigma e^{i\omega_0\tau_0}\Big(-3(g_{u_1u_1}(0,0))^2+3i\omega_0g_{u_1u_1}(0,0)g_{u_1u_2}(0,0)-2\omega_0^2(g_{u_1u_2}(0,0))^2\\
&\quad-\omega_0^2g_{u_1u_1}(0,0)g_{u_2u_2}(0,0)+3i\omega_0^3g_{u_1u_2}(0,0)g_{u_2u_2}(0,0)\Big)\Big],\\
c_{22} &= \frac{2\tau_0D_1g_{u_1u_1}(0,0)}{i\omega_0}\Big[\bar{D}\bar{\sigma}e^{-i\omega_0\tau_0}\Big(g_{u_1u_1}(0,0)+i\omega_0g_{u_1u_2}(0,0)\Big)\\
&\quad+D\sigma e^{i\omega_0\tau_0}\Big(-g_{u_1u_1}(0,0)+i\omega_0g_{u_1u_2}(0,0)\Big)\Big].
\end{aligned}
\tag{5.30}
$$

(*iii*) To compute $Proj_{Ker(M_3^1)}D_yf(x,0,\mu)U_2^2(x,0)$ we define $h=h(x)(\theta)=U_2^2$, and write

$$
h(\theta)=\begin{pmatrix}h^{(1)}(\theta)\\h^{(2)}(\theta)\end{pmatrix}=h_{200}x_1^2+h_{020}x_2^2+h_{002}x_3^2+h_{110}x_1x_2+h_{101}x_1x_3+h_{011}x_2x_3, \tag{5.31}
$$

where $h_{200}, h_{020}, h_{002}, h_{110}, h_{101}, h_{011} \in Q^1$. Then we solve for the coefficients of h using the fact that $(M_2^2 h)(x) = f_2^2(x, 0, 0)$, or equivalently,

$$D_x h J x - \mathcal{A}_{Q^1}(h) = (I - \pi) X_0 F_2(\Phi x, 0). \tag{5.32}$$

Applying the definition of $\mathcal{A}$ and π we obtain the following ordinary differential equation,

$$\begin{aligned} \dot{h} - D_x h J x &= \Phi(\theta)\Psi(0) F_2(\Phi x, 0), \\ \dot{h}(0) - Lh &= F_2(\Phi x, 0), \end{aligned} \tag{5.33}$$

where $\dot{h}$ is the derivative of h with respect to θ. If we denote

$$F_2(\Phi x, 0) = A_{200} x_1^2 + A_{020} x_2^2 + A_{002} x_3^2 + A_{110} x_1 x_2 + A_{101} x_1 x_3 + A_{011} x_2 x_3, \tag{5.34}$$

where $A_{ijk} \in \mathbb{C}^2$, $0 \le i, j, k \le 2, i+j+k = 2$, we are able to compare the coefficients of each monomial and obtain a differential equation for each individual coefficient of h. An inspection of the coefficients in $F_2(\Phi x, 0)$ reveals that $\bar{h}_{020} = h_{200}$ and $\bar{h}_{011} = h_{101}$, and therefore we must only solve the following ordinary differential equations,

$$\begin{cases} \dot{h}_{200} - 2i\omega_0\tau_0 h_{200} = \Phi(\theta)\Psi(0) A_{200}, \\ \dot{h}_{200}(0) - L(h_{200}) = A_{200}, \end{cases} \tag{5.35}$$

$$\begin{cases} \dot{h}_{101} - i\omega_0\tau_0 h_{101} = \Phi(\theta)\Psi(0) A_{101}, \\ \dot{h}_{101}(0) - L(h_{101}) = A_{101}, \end{cases} \tag{5.36}$$

$$\begin{cases} \dot{h}_{110} = \Phi(\theta)\Psi(0) A_{110}, \\ \dot{h}_{110}(0) - L(h_{110}) = A_{110}, \end{cases} \tag{5.37}$$

$$\begin{cases} \dot{h}_{002} = \Phi(\theta)\Psi(0) A_{002}, \\ \dot{h}_{002}(0) - L(h_{002}) = A_{002}. \end{cases} \tag{5.38}$$

The equations for each coefficient in h is solved in full detail in the appendix.

Since

$$F_2(u_t,0)=\begin{pmatrix}0\\ \tau_0 g_{u_1u_1}(0,0)u_1^2(-1)+\tau_0 g_{u_2u_2}(0,0)u_2^2(-1)+2\tau_0 g_{u_1u_2}(0,0)u_1(-1)u_2(-1)\end{pmatrix}, \tag{5.39}$$

we have

$$D_y f_2^1|_{y=0,\mu=0}(h)=\frac{\tau_0}{2}\begin{pmatrix}\psi_{12}H_2(x_1,x_2,x_3)(h)\\ \psi_{22}H_2(x_1,x_2,x_3)(h)\\ \psi_{32}H_2(x_1,x_2,x_3)(h)\end{pmatrix}, \tag{5.40}$$

where

$$\begin{aligned}H_2(x_1,x_2,x_3)(h)=&g_{u_1u_1}(0,0)(e^{-i\omega_0\tau_0}x_1+e^{i\omega_0\tau_0}x_2+x_3)h^{(1)}(-1)+\\ &g_{u_2u_2}(0,0)(i\omega_0e^{-i\omega_0\tau_0}x_1-i\omega_0e^{i\omega_0\tau_0}x_2)h^{(2)}(-1)+g_{u_1u_2}(0,0)(e^{-i\omega_0\tau_0}x_1\\ &+e^{i\omega_0\tau_0}x_2+x_3)h^{(2)}(-1)+g_{u_1u_2}(0,0)(i\omega_0e^{-i\omega_0\tau_0}x_1\\ &-i\omega_0e^{i\omega_0\tau_0}x_2)h^{(1)}(-1).\end{aligned} \tag{5.41}$$

Therefore,

$$Proj_{\mathrm{Ker}(M_3^1)}(D_yf_2^1(x,y,\mu))U_2^2(x,\mu)|_{y=0,\mu=0}=\begin{pmatrix}d_{11}x_1^2x_2+d_{12}x_1x_3^2\\ \bar{d}_{11}x_1x_2^2+\bar{d}_{12}x_2x_3^2\\ d_{21}x_1x_2x_3+d_{22}x_3^3\end{pmatrix}, \tag{5.42}$$

where

$$\begin{aligned}
d_{11} =&\frac{\tau_0\bar{D}\bar{\sigma}}{2}\Big[g_{u_1u_1}(0,0)(e^{i\omega_0\tau_0}h^{(1)}_{200}(-1)+e^{-i\omega_0\tau_0}h^{(1)}_{110}(-1))+g_{u_1u_2}(0,0)(e^{i\omega_0\tau_0}h^{(2)}_{200}(-1)\\
&+e^{-i\omega_0\tau_0}h^{(2)}_{110}(-1)+i\omega_0e^{-i\omega_0\tau_0}h^{(1)}_{110}(-1)-i\omega_0e^{i\omega_0\tau_0}h^{(1)}_{200}(-1))\\
&+i\omega_0g_{u_2u_2}(0,0)(e^{-i\omega_0\tau_0}h^{(2)}_{110}(-1)-e^{i\omega_0\tau_0}h^{(2)}_{200}(-1))\Big],\\
d_{12} =&\frac{\tau_0\bar{D}\bar{\sigma}}{2}\Big[g_{u_1u_1}(0,0)(e^{-i\omega_0\tau_0}h^{(1)}_{002}(-1)+h^{(1)}_{101}(-1))+i\omega_0g_{u_2u_2}(0,0)e^{-i\omega_0\tau_0}h^{(2)}_{002}(-1)\\
&+g_{u_1u_2}(0,0)(e^{-i\omega_0\tau_0}h^{(2)}_{002}(-1)+h^{(2)}_{101}(-1)+i\omega_0e^{-i\omega_0\tau_0}h^{(1)}_{002}(-1))\Big],\\
d_{21} =&\frac{-\tau_0D_1}{2}\Big[g_{u_1u_1}(0,0)(e^{-i\omega_0\tau_0}h^{(1)}_{011}(-1)+e^{i\omega_0\tau_0}h^{(1)}_{101}(-1)+h^{(1)}_{110}(-1))\\
&+i\omega_0g_{u_2u_2}(0,0)(e^{-i\omega_0\tau_0}h^{(2)}_{011}(-1)-e^{i\omega_0\tau_0}h^{(2)}_{101}(-1))+g_{u_1u_2}(0,0)(e^{i\omega_0\tau_0}h^{(2)}_{011}(-1)\\
&+e^{i\omega_0\tau_0}h^{(2)}_{101}(-1)+h^{(2)}_{110}(-1)+i\omega_0e^{-i\omega_0\tau_0}h^{(1)}_{011}(-1)-i\omega_0e^{i\omega_0\tau_0}h^{(1)}_{101}(-1))\Big],\\
d_{22} =&\frac{-\tau_0D_1}{2}\Big[g_{u_1u_1}(0,0)h^{(1)}_{002}(-1)+g_{u_1u_2}(0,0)h^{(2)}_{002}(-1)\Big].
\end{aligned} \tag{5.43}$$

(*iv*) Lastly, to compute $Proj_{Ker(M_3^1)}D_xU_2^1(x,\mu)JU_2^1(x,\mu)$, $Proj_{Ker(M_3^1)}D_xU_2^1(x,\mu)f_2^1(x,0,0)$ and $Proj_{Ker(M_3^1)}(D_xU_2^1(x,0))^2Jx$ we must only use the explicit form of $U_2^1(x,\mu)$ as given in (5.28).

Then,

$$Proj_{\mathrm{Ker}(M_3^1)}D_xU_2^1(x,0)JU_2^1(x,0)=\begin{pmatrix}e_{11}x_1^2x_2+e_{12}x_1x_3^2\\ \bar{e}_{11}x_1x_2^2+\bar{e}_{12}x_2x_3^2\\ e_{21}x_1x_2x_3+e_{22}x_3^3\end{pmatrix}, \tag{5.44}$$

where

$$
\begin{aligned}
e_{11} =& \frac{-2\tau_0^2\bar{D}\bar{\sigma}}{9i\omega_0}\Big[\bar{D}\bar{\sigma}e^{-i\omega_0\tau_0}(27(g_{u_1u_1}(0,0))^2e^{-i\omega_0\tau_0} - 27\omega_0^4(g_{u_2u_2}(0,0))^2e^{-i\omega_0\tau_0} \\
&+ 18i\omega_0 g_{u_1u_1}(0,0)g_{u_1u_2}(0,0)e^{-i\omega_0\tau_0} + 18i\omega_0^3 g_{u_1u_2}(0,0)g_{u_2u_2}(0,0)e^{-i\omega_0\tau_0} + \\
&36i\omega_0 g_{u_1u_1}(0,0)g_{u_1u_2}(0,0) + 36i\omega_0^3 g_{u_1u_2}(0,0)g_{u_2u_2}(0,0)) + D\sigma(-19(g_{u_1u_1}(0,0))^2 \\
&- 34\omega_0^2 g_{u_1u_1}(0,0)g_{u_2u_2}(0,0) - 19\omega_0^4(g_{u_2u_2}(0,0))^2 - 4\omega_0^2(g_{u_1u_2}(0,0))^2)\Big], \\
e_{12} =& \frac{-\tau_0^2\bar{D}\bar{\sigma}}{i\omega_0}\Big[\bar{D}\bar{\sigma}e^{-i\omega_0\tau_0}(2(g_{u_1u_1}(0,0))^2e^{-i\omega_0\tau_0} + 4i\omega_0 g_{u_1u_1}(0,0)g_{u_1u_2}(0,0) \\
&- 2\omega_0^2 g_{u_1u_1}(0,0)g_{u_2u_2}(0,0)e^{-i\omega_0\tau_0}) + D\sigma(-3(g_{u_1u_1}(0,0))^2 \\
&- 2\omega_0^2 g_{u_1u_1}(0,0)g_{u_2u_2}(0,0) - \omega_0^2(g_{u_1u_2}(0,0))^2)\Big], \\
e_{21} =& \frac{\tau_0^2 D_1}{i\omega_0}\Big[\bar{D}\bar{\sigma}e^{-i\omega_0\tau_0}(5(g_{u_1u_1}(0,0))^2 + 3\omega_0^2 g_{u_1u_1}(0,0)g_{u_2u_2}(0,0) \\
&+ 5i\omega_0^3 g_{u_1u_2}(0,0)g_{u_2u_2}(0,0) + 5i\omega_0 g_{u_1u_1}(0,0)g_{u_1u_2}(0,0) + 2\omega_0^2(g_{u_1u_2}(0,0))^2) \\
&- D\sigma e^{i\omega_0\tau_0}(5(g_{u_1u_1}(0,0))^2 + 3\omega_0^2 g_{u_1u_1}(0,0)g_{u_2u_2}(0,0) - 5i\omega_0^3 g_{u_1u_2}(0,0)g_{u_2u_2}(0,0) \\
&- 5i\omega_0 g_{u_1u_1}(0,0)g_{u_1u_2}(0,0) + 2\omega_0^2(g_{u_1u_2}(0,0))^2)\Big], \\
e_{22} =& \frac{2\tau_0^2 D_1 g_{u_1u_1}(0,0)}{i\omega_0}\Big[\bar{D}\bar{\sigma}e^{-i\omega_0\tau_0}(g_{u_1u_1}(0,0) + i\omega_0 g_{u_1u_2}(0,0)) - D\sigma e^{i\omega_0\tau_0}(g_{u_1u_1}(0,0) \\
&- i\omega_0 g_{u_1u_2}(0,0))\Big].
\end{aligned}
\tag{5.45}
$$

Similarly,

$$
Proj_{\mathrm{Ker}(M_3^1)}D_xU_2^1(x,0)f_2^1(x,0,0) = \begin{pmatrix} f_{11}x_1^2x_2 + f_{12}x_1x_3^2 \\ \bar{f}_{11}x_1x_2^2 + \bar{f}_{12}x_2x_3^2 \\ f_{21}x_1x_2x_3 + f_{22}x_3^3 \end{pmatrix}, \tag{5.46}
$$

where

$$
\begin{aligned}
f_{11} =& \frac{-\tau_0^2 \bar{D}\bar{\sigma}}{3i\omega}\Big[\bar{D}\bar{\sigma}e^{-i\omega_0\tau_0}(-6(g_{u_1u_1}(0,0))^2e^{-i\omega_0\tau_0} + 12i\omega_0 g_{u_1u_1}(0,0)g_{u_1u_2}(0,0)e^{-i\omega_0\tau_0} \\
&+ 6\omega_0^4(g_{u_2u_2}(0,0))^2e^{-i\omega_0\tau_0} + 12i\omega_0^3 g_{u_1u_2}(0,0)g_{u_2u_2}(0,0)e^{-i\omega_0\tau_0} \\
&- 24i\omega_0^3 g_{u_1u_2}(0,0)g_{u_2u_2}(0,0) - 24i\omega_0 g_{u_1u_1}(0,0)g_{u_1u_2}(0,0)) + D\sigma(14(g_{u_1u_1}(0,0))^2 \\
&+ 20\omega_0^2 g_{u_1u_1}(0,0)g_{u_2u_2}(0,0) + 14\omega_0^4(g_{u_2u_2}(0,0))^2 + 8\omega_0^2(g_{u_1u_2}(0,0))^2) \\
&+ D_1e^{-i\omega_0\tau_0}(-3(g_{u_1u_1}(0,0))^2 - 3i\omega_0 g_{u_1u_2}(0,0)g_{u_2u_2}(0,0) + 3\omega_0^2 g_{u_1u_1}(0,0)g_{u_2u_2}(0,0) \\
&- 3i\omega_0 g_{u_1u_1}(0,0)g_{u_1u_2}(0,0) - 6\omega_0(g_{u_1u_2}(0,0))^2)\Big], \\
f_{12} =& \frac{2\tau_0 \bar{D}\bar{\sigma}}{i\omega_0}\Big[\bar{D}\bar{\sigma}e^{-i\omega_0\tau_0}((g_{u_1u_1}(0,0))^2e^{-i\omega_0\tau_0} + 2i\omega_0 g_{u_1u_1}(0,0)g_{u_1u_2}(0,0) \\
&- \omega_0^2 g_{u_1u_1}(0,0)g_{u_2u_2}(0,0)e^{-i\omega_0\tau_0})) + D\sigma(-2(g_{u_1u_1}(0,0))^2 - \omega_0^2 g_{u_1u_1}(0,0)g_{u_2u_2}(0,0) \\
&- \omega_0^2(g_{u_1u_2}(0,0))^2) + D_1e^{-i\omega_0\tau_0}(2(g_{u_1u_1}(0,0))^2 + 2i\omega_0 g_{u_1u_1}(0,0)g_{u_1u_2}(0,0))\Big], \\
f_{21} =& \frac{-2\tau_0^2 D_1}{i\omega_0}\Big[\bar{D}\bar{\sigma}e^{-i\omega_0\tau_0}(3(g_{u_1u_1}(0,0))^2 + \omega_0^2 g_{u_1u_1}(0,0)g_{u_2u_2}(0,0) \\
&+ 3i\omega_0^3 g_{u_1u_2}(0,0)g_{u_2u_2}(0,0) + 2\omega_0^2(g_{u_1u_2}(0,0))^2 + 3i\omega_0 g_{u_1u_1}(0,0)g_{u_1u_2}(0,0)) \\
&- D\sigma e^{i\omega_0\tau_0}(3(g_{u_1u_1}(0,0))^2 + \omega_0^2 g_{u_1u_1}(0,0)g_{u_2u_2}(0,0) - 3i\omega_0^3 g_{u_1u_2}(0,0)g_{u_2u_2}(0,0) \\
&+ 2\omega_0^2(g_{u_1u_2}(0,0))^2 - 3i\omega_0 g_{u_1u_1}(0,0)g_{u_1u_2}(0,0))\Big], \\
f_{22} =& \frac{-2\tau_0^2 D_1 g_{u_1u_1}(0,0)}{i\omega_0}\Big[\bar{D}\bar{\sigma}e^{-i\omega_0\tau_0}(g_{u_1u_1}(0,0) + i\omega_0 g_{u_1u_2}(0,0)) - D\sigma e^{i\omega_0\tau_0}(g_{u_1u_1}(0,0) \\
&- i\omega_0 g_{u_1u_2}(0,0))\Big].
\end{aligned}
\tag{5.47}
$$

And finally,

$$
Proj_{\mathrm{Ker}(M_3^1)}(D_xU_2^1(x,0))^2Jx = \begin{pmatrix} g_{11}x_1^2x_2 + g_{12}x_1x_3^2 \\ \bar{g}_{11}x_1x_2^2 + \bar{g}_{12}x_2x_3^2 \\ g_{21}x_1x_2x_3 + g_{22}x_3^3 \end{pmatrix}, \tag{5.48}
$$

where

$$
\begin{aligned}
g_{11} =&\frac{-\tau_0^2\bar{D}\bar{\sigma}}{9i\omega_0}\Big[\bar{D}\bar{\sigma}e^{-i\omega_0\tau_0}(36(g_{u_1u_1}(0,0))^2e^{-i\omega_0\tau_0}+72i\omega_0 g_{u_1u_1}(0,0)g_{u_1u_2}(0,0)\\
&+72i\omega_0^3 g_{u_1u_2}(0,0)g_{u_2u_2}(0,0)-36\omega_0^4(g_{u_2u_2}(0,0))^2e^{-i\omega_0\tau_0})+D\sigma(4(g_{u_1u_1}(0,0))^2\\
&-8\omega_0^2 g_{u_1u_1}(0,0)g_{u_2u_2}(0,0)+4\omega_0^4(g_{u_2u_2}(0,0))^2+16\omega_0^2(g_{u_1u_2})^2)\\
&+D_1e^{-i\omega_0\tau_0}(-9(g_{u_1u_1}(0,0))^2-9i\omega_0 g_{u_1u_1}(0,0)g_{u_1u_2}(0,0)+9\omega_0^2 g_{u_1u_1}(0,0)g_{u_2u_2}(0,0)\\
&-9i\omega_0^3 g_{u_1u_2}(0,0)g_{u_2u_2}(0,0)-18\omega_0^2(g_{u_1u_2}(0,0))^2)\Big]\\
g_{12} =&\frac{\tau_0^2\bar{D}\bar{\sigma}}{i\omega_0}\Big[D\sigma((g_{u_1u_1}(0,0))^2+\omega_0^2(g_{u_1u_2}(0,0))^2)+D_1g_{u_1u_1}(0,0)e^{-i\omega_0\tau_0}(-4g_{u_1u_1}(0,0)\\
&-4i\omega_0 g_{u_1u_2}(0,0))\Big]\\
g_{21} =&\frac{\tau_0^2D_1}{i\omega_0}\Big[\bar{D}\bar{\sigma}e^{-i\omega_0\tau_0}((g_{u_1u_1}(0,0))^2+i\omega_0 g_{u_1u_1}(0,0)g_{u_1u_2}(0,0)-\omega_0^2 g_{u_1u_1}(0,0)g_{u_2u_2}(0,0)\\
&+i\omega_0^3 g_{u_1u_2}(0,0)g_{u_2u_2}(0,0)+2\omega_0^2(g_{u_1u_2})^2)-D\sigma e^{i\omega_0\tau_0}(g_{u_1u_1}(0,0))^2\\
&-i\omega_0 g_{u_1u_1}(0,0)g_{u_1u_2}(0,0)-\omega_0^2 g_{u_1u_1}(0,0)g_{u_2u_2}(0,0)-i\omega_0^3 g_{u_1u_2}(0,0)g_{u_2u_2}(0,0)\\
&+2\omega_0^2(g_{u_1u_2})^2)\Big]\\
g_{22} =&0
\end{aligned}
\tag{5.49}
$$

Therefore, on the centre manifold, System (5.19) can be reduced to

$$
\begin{cases}
\dot{x_1} =i\omega_0x_1+(a_{11}\mu_1+a_{12}\mu_2)x_1+a_{13}x_1x_3+(b_{11}+c_{11}+d_{11}-e_{11}-f_{11}+g_{11})x_1^2x_2\\
\qquad+(b_{12}+c_{12}+d_{12}-e_{12}-f_{12}+g_{12})x_1x_3^2+h.o.t.,\\
\dot{x_2} =-i\omega_0x_2+(\bar{a}_{11}\mu_1+\bar{a}_{12}\mu_2)x_2+\bar{a}_{13}x_2x_3+(\bar{b}_{11}+\bar{c}_{11}+\bar{d}_{11}-\bar{e}_{11}-\bar{f}_{11}+\bar{g}_{11})x_1x_2^2\\
\qquad+(\bar{b}_{12}+\bar{c}_{12}+\bar{d}_{12}-\bar{e}_{12}-\bar{f}_{12}+\bar{g}_{12})x_2x_3^2+h.o.t.,\\
\dot{x_3} =(a_{21}\mu_1+a_{22}\mu_2)x_3+a_{23}x_3^2+(b_{21}+c_{21}+d_{21}-e_{21}-f_{21}+g_{21})x_1x_2x_3\\
\qquad+(b_{22}+c_{22}+d_{22}-e_{22}-f_{22}+g_{22})x_3^3+h.o.t.
\end{cases}
\tag{5.50}
$$

We can convert the above ODE from complex variables to real variables by introducing

the change of variables $x_1 = w_1 - iw_2$, $x_2 = w_1 + iw_2$, $x_3 = w_3$. Upon completing this change of variables we may now convert to cylindrical coordinates by letting $w_1 = r\cos\xi$, $w_2 = r\sin\xi$, $w_3 = z$. System (5.50) now becomes

$$\begin{cases} \dot{r} = \alpha_1(\mu)r + \beta_{11}rz + \beta_{30}r^3 + \beta_{12}rz^2 + h.o.t., \\ \dot{z} = \alpha_2(\mu)z + \gamma_{20}r^2 + \gamma_{02}z^2 + \gamma_{03}z^3 + h.o.t., \\ \dot{\xi} = -\omega_0 + (\mathrm{Im}[a_{11}]\mu_1 + \mathrm{Im}[a_{12}]\mu_2)r + h.o.t., \end{cases} \tag{5.51}$$

where

$$\begin{aligned} &\alpha_1(\mu) = \mathrm{Re}[a_{11}]\mu_1 + \mathrm{Re}[a_{12}]\mu_2,\ \alpha_2(\mu) = a_{21}\mu_1 + a_{22}\mu_2,\ \beta_{11} = \mathrm{Re}[a_{13}], \\ &\beta_{30} = \mathrm{Re}[b_{11} + c_{11} + d_{11} - e_{11} - f_{11} + g_{11}],\ \beta_{12} = \mathrm{Re}[b_{12} + c_{12} + d_{12} - e_{12} - f_{12} + g_{12}], \\ &\gamma_{20} = a_{23}, \quad \gamma_{02} = a_{24},\ \gamma_{21} = b_{21} + c_{21} + d_{21} - e_{21} - f_{21} + g_{21}, \\ &\gamma_{03} = b_{22} + c_{22} + d_{22} - e_{22} - f_{22} + g_{22}. \end{aligned} \tag{5.52}$$

Chapter 6

Bifurcation Diagrams

In this chapter we will determine the bifurcation diagrams for (5.51) based on values of the bifurcation parameters μ_1 and μ_2. We draw direct links between the normal form found in the previous chapter and the normal form of the Zero-Hopf bifurcation as it is given in [6] and in Chapter 3 of this thesis. This will allow us to accurately predict the behaviour of the system on the centre manifold for any given initial conditions of the system.

Dropping the azimuthal component of the normal form, we have

$$\begin{aligned} \dot{r} =& \alpha_1(\mu) r + \beta_{11} r z + \beta_{30} r^3 + \beta_{12} r z^2, \\ \dot{z} =& \alpha_2(\mu) z + \gamma_{20} r^2 + \gamma_{02} z^2 + \gamma_{03} z^3, \end{aligned} \tag{6.1}$$

where the coefficients are as they are defined in (5.52). To achieve the exact normal form of the Zero-Hopf bifurcation we let $r \to r$ and $z \to z + \delta$, where δ is yet to be defined explicitly. This gives

$$\begin{aligned} \dot{r} =& (\alpha_1(\mu) + \beta_{11}\delta + \beta_{12}\delta^2) r + (\beta_{11} + 2\delta\beta_{12}) r z + \beta_{30} r^3 + \beta_{12} r z^2, \\ \dot{z} =& (\alpha_2(\mu)\delta + \gamma_{02}\delta^2 + \gamma_{03}\delta^3) + (\alpha_2(\mu) + 2\delta\gamma_{02} + 3\gamma_{03}\delta^2) z + \gamma_{02} r^2 + (\gamma_{02} + 3\delta) z^2 + \gamma_{03} z^3. \end{aligned} \tag{6.2}$$

We choose $\delta = \delta(\mu)$ such that $(\alpha_2(\mu) + 2\delta\gamma_{02} + 3\gamma_{03}\delta^2) = 0$. Therefore,

$$\begin{aligned}\delta(\mu) =& \frac{1}{3\gamma_{03}}\Big[-\gamma_{02} \pm \sqrt{\gamma_{02}^2 - 3\gamma_{03}\alpha_2(\mu)}\Big] \\ =& \frac{1}{3\gamma_{03}}\Big[-a_{24} \pm \sqrt{a_{24}^2 - 3\gamma_{03}a_{21}\mu_1}\Big].\end{aligned} \tag{6.3}$$

Now to ensure $\delta(0) = 0$ we choose

$$\delta(\mu_1) = \begin{cases} \dfrac{1}{3\gamma_{03}}\Big[-a_{24} + \sqrt{a_{24}^2 - 3\gamma_{03}a_{21}\mu_1}\Big], & a_{24} \geq 0, \\ \\ \dfrac{1}{3\gamma_{03}}\Big[-a_{24} - \sqrt{a_{24}^2 - 3\gamma_{03}a_{21}\mu_1}\Big], & a_{24} < 0. \end{cases} \tag{6.4}$$

For small values of μ_1, δ is a continuous function that is differentiable at $\mu_1 = 0$. Letting

$$\begin{aligned}&\eta_1 = \alpha_1(\mu) + \beta_{11}\delta + \beta_{12}\delta^2, \quad a_1 = \beta_{11} + 2\delta\beta_{12}, \quad a_2 = \beta_{30}, \quad a_3 = \beta_{12} \\ &\eta_2 = \alpha_2(\mu)\delta + 2\gamma_{02}\delta^2 + \gamma_{03}\delta^3, \quad b_1 = \gamma_{20}, \quad b_2 = \gamma_{02} + 3\delta,\end{aligned} \tag{6.5}$$

we obtain the normal form of the Zero-Hopf bifurcation as given in (3.2).

Provided that a_1, b_1 and b_2 are nonzero, we may only consider terms up to the second order. Upon tracing the values back to equation (5.22) the non degenerate conditions can be simplified by ensuring $g_{u_1u_1}(0,0) \neq \omega_0^2 g_{u_2u_2}(0,0)$ and $g_{u_1u_1}(0,0) \neq 0$. Then truncating the system at the second order gives us

$$\begin{aligned}\dot{r} =& \eta_1 r + a_1 r z, \\ \dot{z} =& \eta_2 + b_1 r^2 + b_2 z^2.\end{aligned} \tag{6.6}$$

Now taking $r \to -\sqrt{|b_1 b_2|}r$ and $z \to -b_2 z$, we get

$$\begin{aligned}\dot{r} =& \chi_1 r + A r z, \\ \dot{z} =& \chi_2 + B r^2 - z^2,\end{aligned} \tag{6.7}$$

where

$$\begin{aligned}\chi_1 = \eta_1, \quad A = \frac{-a_1}{b_2}, \\ \chi_2 = -b_2\eta_2, \quad B = \pm 1.\end{aligned} \tag{6.8}$$

Recall from the previous work on the Zero-Hopf bifurcation that when $B = 1$ (respectively $B = -1$) and $A > 0$ ($A < 0$) the bifurcation diagrams in the (χ_1, χ_2)-plane contain the origin and the curves

$$\begin{aligned} S &= \big\{(\chi_1, \chi_2) : \chi_2 = 0, \chi_1 \neq 0\big\}, \\ P &= \left\{(\chi_1, \chi_2) : \chi_2 = \frac{1}{A^2}\chi_1^2 + \mathcal{O}(|\chi_1|^3), \chi_1 \neq 0\right\}, \end{aligned} \tag{6.9}$$

where a saddle-node bifurcation and pitchfork bifurcation occur respectively.

Furthermore, when $B = 1$ (respectively $B = -1$) and $A < 0$ ($A > 0$) the bifurcation diagrams in the (χ_1, χ_2)-plane contain the origin, the curves P and S and the curves

$$\begin{aligned} M &= \big\{(\chi_1, \chi_2) : \chi_1 = 0, \chi_2 < 0 \ (\chi_2 > 0)\big\}, \\ N &= \left\{(\chi_1, \chi_2) : \chi_1 = \frac{-A}{3A+2}\chi_2 + \mathcal{O}(|\chi_2|^{\frac{3}{2}}), \chi_2 < 0 \ (\chi_2 > 0)\right\}, \end{aligned} \tag{6.10}$$

where Hopf and Cycle Blow-up (Heteroclinic) bifurcations are occurring respectively.

We now work to define these bifurcation diagrams in terms of the bifurcation parameters μ_1 and μ_2. We start by using the fact that δ is differentiable at 0 and $\delta(0) = 0$ to obtain the Taylor series expansion

$$\delta(\mu_1) = \frac{-a_{21}}{2a_{24}}\mu_1 - \frac{3a_{21}^2\gamma_{03}}{8a_{24}^2}\mu_1^2 + \mathcal{O}(|\mu_1|^3). \tag{6.11}$$

We also find that

$$A = \frac{-a_1}{b_2} = \frac{-\beta_{11} - \delta\beta_{12}}{\gamma_{02}} = \frac{-\mathrm{Re}[a_{13}]}{\gamma_{02}} + \mathcal{O}(|\mu_1|). \tag{6.12}$$

And finally,

$$\begin{aligned} \chi_1 &= -b_2(\alpha_2(\mu)\delta + 2\gamma_{02}\delta^2 + \gamma_{03}\delta^3) \\ &= \frac{(2a_{24}\mathrm{Re}[a_{11}] - a_{21}\mathrm{Re}[\mathrm{a}_{13}])}{2a_{24}}\mu_1 + \mathrm{Re}[a_{12}]\mu_2 + \frac{a_{21}^2(2\beta_{12} - 3a_{24}\mathrm{Re}[a_{13}])}{8a_{24}^2}\mu_1^2 + \mathcal{O}(|\mu_1|^3), \\ \chi_2 &= \alpha_1(\mu) + \beta_{11}\delta + \beta_{12}\delta^2 \\ &= \frac{-a_{21}^3\gamma_{03}}{8a_{24}^2}\mu_1^3 + \mathcal{O}(|\mu_1|^4). \end{aligned} \tag{6.13}$$

This now brings us to the following theorem about the bifurcation diagrams in the (μ_1, μ_2)-plane.

Theorem 6.1. *Let $(\mu_1, \mu_2) \neq (0,0)$ be sufficiently small, $g_{u_1u_1}(0,0) \neq -g_{u_2u_2}(0,0)$ and $g_{u_1u_1}(0,0) \neq 0$. Then for A and B defined above we have the following.*
(a) If $B = 1$ (respectively $B = -1$) and $A > 0$ ($A < 0$) then the bifurcation diagram of System (5.4) contains the origin and the curves

$$S = \{(\mu_1, \mu_2) : \mu_1 = 0, \mu_2 \neq 0\},$$
$$P = \left\{(\mu_1, \mu_2) : \mu_2 = \frac{(a_{21}\mathrm{Re}[a_{13}] - 2a_{24}\mathrm{Re}[a_{11}])}{2\mathrm{Re}[a_{12}]a_{24}}\mu_1 \pm \frac{\mathrm{Re}[a_{13}]a_{21}}{2\mathrm{Re}[a_{12}]a_{24}^2}\sqrt{\frac{-a_{21}\gamma_{03}\mu_1^3}{2}},\right.$$
$$\left. a_{21}\gamma_{03}\mu_1 < 0\right\},$$

where saddle-node and pitchfork bifurcations are occurring respectively.
(b) If $B = 1$ (respectively $B = -1$) and $A < 0$ ($A > 0$) then the bifurcation diagram of System (5.4) contains the origin, the curves S, P as defined in (a) and the curves

$$M = \left\{(\mu_1, \mu_2) : \mu_2 = \frac{(a_{21}\mathrm{Re}[a_{13}] - 2a_{24}\mathrm{Re}[a_{11}])}{2\mathrm{Re}[a_{12}]a_{24}}\mu_1, a_{21}\gamma_{03}\mu_1 > 0 \ (a_{21}\gamma_{03}\mu_1 < 0)\right\},$$
$$N = \left\{(\mu_1, \mu_2) : \mu_2 = \frac{(a_{21}\mathrm{Re}[a_{13}] - 2a_{24}\mathrm{Re}[a_{11}])}{2\mathrm{Re}[a_{12}]a_{24}}\mu_1 + \frac{a_{21}(3a_{24}\mathrm{Re}[a_{13}] - 2\beta_{12})}{8a_{24}^2\mathrm{Re}[a_{12}]}\mu_1^2\right.$$
$$\left. + \frac{a_{21}^3\mathrm{Re}[a_{13}]\gamma_{03}}{a_{24}^2(3\mathrm{Re}[a_{13}] - 2a_{24})}\mu_1^3, a_{21}\gamma_{03}\mu_1 > 0 \ (a_{21}\gamma_{03}\mu_1 < 0)\right\}.$$

Along S and P, the same bifurcations are occurring as in (a). Along M and N, Hopf and Cycle Blow-up (Heteroclinic) bifurcations are occurring respectively.

Chapter 7

Numerical Simulations

Here we work to apply the theoretical results from the previous chapters to the system in (5.4) to confirm our results. This will allow us to bring physical meaning to the bifurcation diagrams given by Guckenheimer and Homes in [6], and help us to understand the dynamics of the system under certain initial conditions. Here we focus on three main phenomena that can be observed in the system; an unstable limit cycle that repels the orbits into a nontrivial fixed point, a stable limit cycle that will attract all orbits on the centre manifold and a stable torus formed by the Hopf bifurcation that occurs in the system.

We use a computer program to effectively project orbits onto the three-dimensional centre manifold and convert them to cylindrical coordinates. Upon doing so, we are able to create phase portraits that closely resemble those given for the Zero-Hopf bifurcation. The code for this program is given in the appendix, and to the author's knowledge, it is an entirely original idea to present the findings in such a way. We will use this program to better understand the nature of the system on the three-dimensional centre manifold and to aid us in understanding the bifurcation taking place.

7.1 Simulation 1: The Nontrivial Fixed Point

Here we take $\varepsilon = 0.6$, $a = 0.5$ and

$$g(u_1, u_2) = au_2 + bu_1 + \frac{1}{20}u_1^2 - \frac{1}{10}u_1u_2 + \frac{1}{4}u_2^2 - \frac{1}{6}u_1^3 + \frac{1}{4}u_1^2u_2 - \frac{1}{4}u_1u_2^2 + \frac{1}{6}u_2^3. \quad (7.1)$$

Clearly, $0 \neq g_{u_1u_1}(0,0) = \frac{1}{10} \neq \omega_0^2 g_{u_2u_2}(0,0) = -0.687385$, and therefore we may apply Theorem 6.1.

Now, $\omega_0 = 1.37477$ and $\tau_0 = 2.17954$. Then from our work in Chapter 5 we get

$$\begin{gathered}
a_{11} = 0.8231 + 0.6314i,\ a_{12} = 1.64586 + 0.83988i,\ a_{13} = 0.16911 - 0.05002i,\\
a_{21} = 2.01895,\ a_{22} = 0,\ a_{23} = 3.95283,\ a_{24} = 0.10094,\ b_{11} = -0.12766 + 0.00519i,\\
b_{12} = -0.90846 + 0.81959i,\ b_{21} = -3.29089,\ b_{22} = -0.33649,\ c_{11} = 1.23482 + 2.29565i,\\
c_{12} = 0.04175 - 0.12696i,\ c_{21} = 1.48191,\ c_{22} = 0.01348,\ d_{11} = 0.2703 + 0.58346i,\\
d_{12} = -0.06815 + 0.06913i,\ d_{21} = -0.16386,\ d_{22} = -0.04387,\ e_{11} = 3.76587 - 5.00276i,\\
e_{12} = 0.11072 - 0.26002i,\ e_{21} = -1.81909,\ e_{22} = 0.02938,\ f_{11} = -0.71929 + 5.47011i,\\
f_{12} = -0.08599 + 0.37121i,\ f_{21} = -1.4819,\ f_{22} = -0.02938,\ g_{11} = 2.53105 - 1.19093i,\\
g_{12} = -0.02938 - 0.12196i,\ g_{21} = 0.43392,\ g_{22} = 0.
\end{gathered} \quad (7.2)$$

This gives us that $B = -1$, $A < 0$ and

$$P = \{(\mu_1, \mu_2) : \mu_2 = 0.5274\mu_1 \pm 6.19443\mu_1^{3/2}\}. \quad (7.3)$$

Choosing $\mu_1 = 0.002$ and $\mu_2 = 0.00095$, this gives us that $b = 1.002$ and $\tau = 2.18049$, and furthermore, we have that the point (μ_1, μ_2) lies between the branches of P in Theorem 6.1.

Figure 7.1 shows the trajectory of the system that is approaching the fixed point at $x \approx 0.3357$. We see that the radius of the trajectory is increasing as it progresses from left to right due to the unstable limit cycle shown in the bifurcation diagrams and as the trajectory become sufficiently close to the cycle, it is thrust towards the

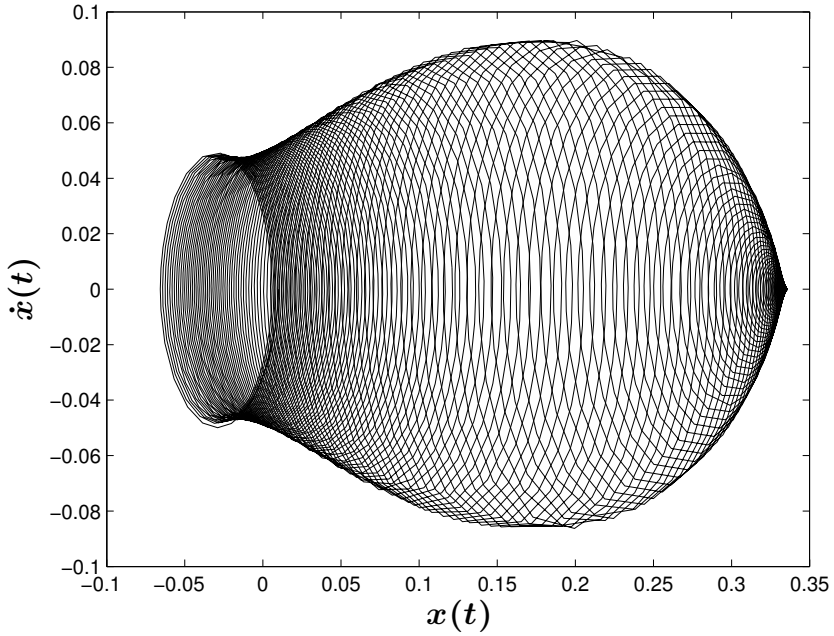

Figure 7.1: An unstable limit cycle bringing trajectories close then pushing them towards a nontrivial fixed point at approximately $x = 0.3357$.

nontrivial fixed point. This phenomenon is better observed in Figure 7.2 where we have plotted multiple trajectories and projected them onto the centre manifold and then converted to cylindrical coordinates and compared it with the original phase portrait predicted in Chapter 3. This shows us the effect of the saddle point (a limit cycle in the original system) pulling trajectories close to it before they are pushed away to the nontrivial fixed point. This phase diagram corresponds exactly with the theoretical results found in [6, 10].

Since the limit cycle is unstable, this tells us that depending on our choice of initial conditions, we may obtain a solution that diverges. That is, a trajectory will not go to an equilibrium. This can be observed in Figure 7.2*b* in the lower and rightmost regions of the phase diagram. This illustrates just one of the many trajectories possible in the system depending on the initial conditions.

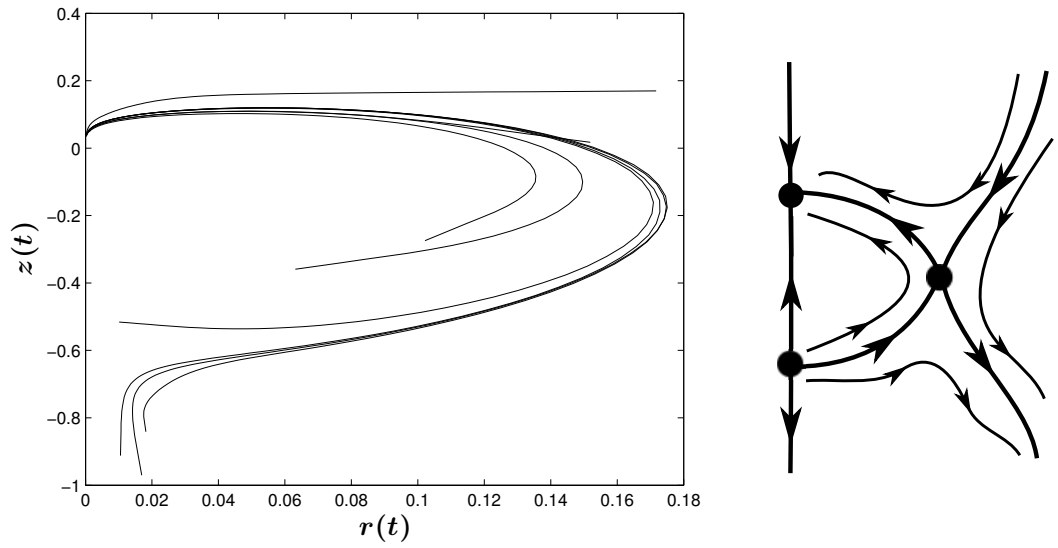

(a) (b)

Figure 7.2: (a) Multiple trajectories projected onto the centre manifold and converted to cylindrical coordinates and (b) the phase portrait predicted in Chapter 3.

7.2 Simulation 2: The Stable Limit Cycle

As a second simulation to confirm our theoretical results we take $\varepsilon = 1$, $a = 0.2$ and

$$g(u_1, u_2) = au_2 + bu_1 - \frac{1}{10}u_1^2 - \frac{1}{2}u_1u_2 + \frac{1}{4}u_2^2 - \frac{1}{6}u_1^3 + \frac{1}{4}u_1^2u_2 - \frac{1}{4}u_1u_2^2 + \frac{1}{6}u_2^3. \quad (7.4)$$

Again, $0 \neq g_{u_1u_1}(0,0) = \frac{-1}{5} \neq 0.5099 = \omega_0^2 g_{u_1u_2}(0,0)$, and we may use the results from Theorem 6.1.

Now, $\omega_0 = 1.0198$, $\tau_0 = 1.77603$ and from the work in Chapter 5 we get,

$a_{11} = -1.15318 - 1.40417i,\ a_{12} = -1.67184 + 1.90376i,\ a_{13} = -0.48535 + 0.86884i,$

$a_{21} = 3.08323,\ a_{22} = 0,\ a_{23} = 1.5887,\ a_{24} = -0.30832,\ b_{11} = -2.43052 + 1.87786i,$

$b_{12} = -0.05886 - 1.49675i,\ b_{21} = -4.15208,\ b_{22} = -0.51387,\ c_{11} = -1.19747 + 0.838i,$

$c_{12} = -1.36241 - 2.50986i,\ c_{21} = 2.27535,\ c_{22} = 1.18324,\ d_{11} = -6.40189 + 7.9301i,$

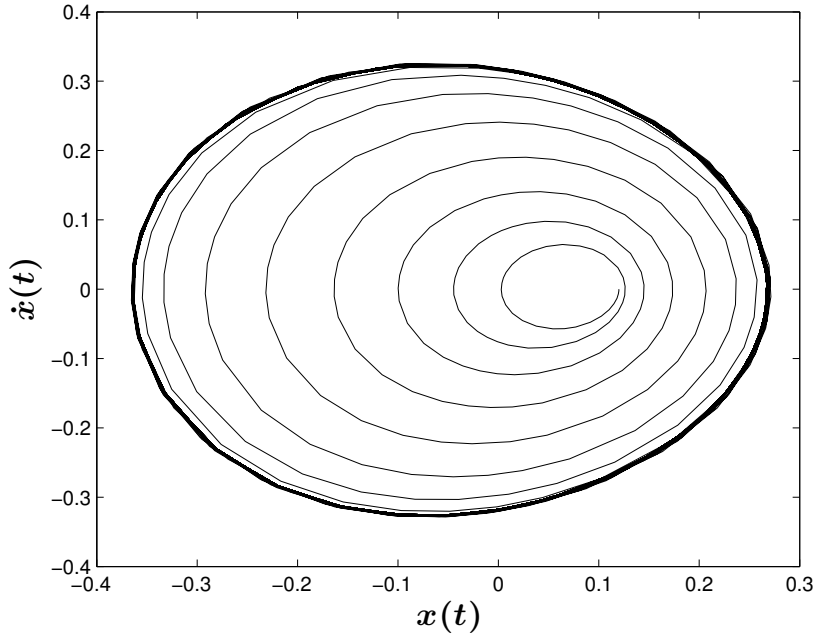

Figure 7.3: A stable limit cycle in the system for $(\mu_1, \mu_2) = (-0.02, 0.0495)$.

$$d_{12} = 0.59595 + 3.64596i,\ d_{21} = -0.40332,\ d_{22} = -1.47911,\ e_{11} = 0.148719 - 1.2894i,$$
$$e_{12} = 0.28244 - 0.18031i,\ e_{21} = 15.47006,\ e_{22} = 2.10146,\ f_{11} = 4.24192 + 5.29266i,$$
$$f_{12} = 1.84226 + 2.33629i,\ f_{21} = -2.27535,\ f_{22} = -2.10146,\ g_{11} = 1.34619 - 1.97031i,$$
$$g_{12} = -2.10146 - 2.14514i,\ g_{21} = 4.50001,\ g_{22} = 0. \tag{7.5}$$

This gives us $B = 1$, $A < 0$ and

$$M = \{(\mu_1, \mu_2) : \mu_2 = -2.14132\mu_1,\ \mu_1 < 0\}. \tag{7.6}$$

Choosing $\mu_1 = -0.02$ and $\mu_2 = 0.0495$, the point (μ_1, μ_2) lies above the curve M, and therefore is between M and S.

As predicted by the bifurcation diagrams of the Zero-Hopf bifurcation, Figure 7.3 shows the existence of a stable limit cycle that will attract all orbits on the centre

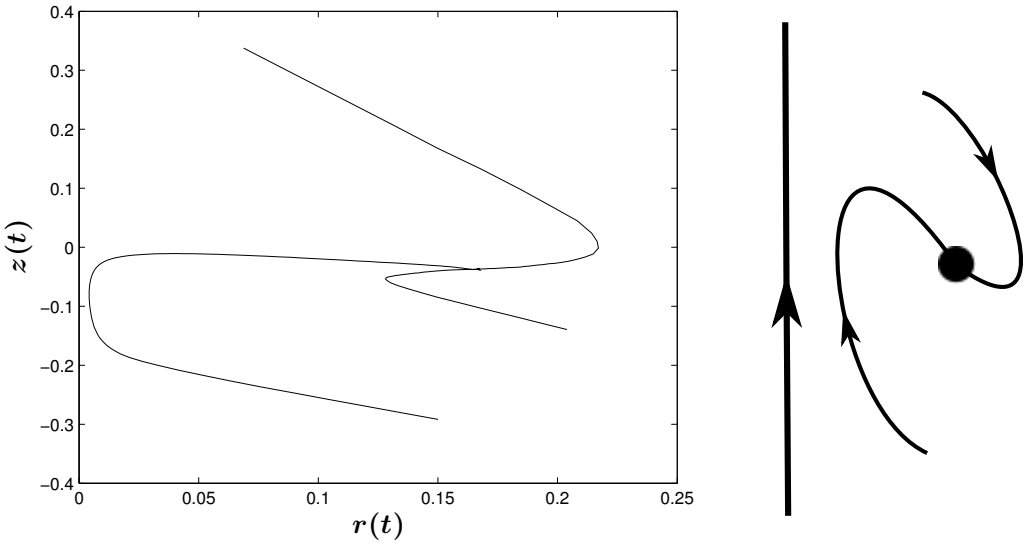

(a) (b)

Figure 7.4: (a) Multiple trajectories projected onto the centre manifold and converted to cylindrical coordinates and (b) the phase portrait predicted in Chapter 3. The fixed point that trajectories converge to relates to a limit cycle in the original system.

manifold. Furthermore, these claims are proven true by Figure 7.4, where trajectories have been projected onto the centre manifold and converted to cylindrical coordinates to reveal the phase portrait. This phase portrait corresponds exactly with that of Guckenheimer and Holmes in [6].

7.3 Simulation 3: The Invariant Torus

Here we explore some of the most interesting dynamics of the Zero-Hopf bifurcation: the invariant torus - a two-dimensional invariant donut shaped manifold existing in a three-dimensional space. We start by taking $\varepsilon = 1.8$, $a = 1.3$ and

$$g(u_1, u_2) = au_2 + bu_1 - \frac{1}{10}u_1^2 - \frac{1}{2}u_1u_2 + \frac{1}{4}u_2^2 - \frac{1}{6}u_1^3 + \frac{1}{4}u_1^2u_2 - \frac{1}{4}u_1u_2^2 + \frac{1}{6}u_2^3. \quad (7.7)$$

This is the same function we used in the second simulation, and therefore we may apply the results from Theorem 6.1 to our simulations.

Now, $\omega_0 = 0.67082$, $\tau_0 = 2.77354$ and again we have,

$$\begin{aligned}
&a_{11} = -0.03403 - 0.90854i,\ a_{12} = -0.62938 + 0.16216i,\ a_{13} = 0.31154 + 0.17029i,\\
&a_{21} = -8.4958,\ a_{22} = 0,\ a_{23} = -2.54875,\ a_{24} = 0.84958,\ b_{11} = 0.1633 - 1.80842i,\\
&b_{12} = 0.43777 - 0.76592i,\ b_{21} = 9.77022,\ b_{22} = 1.41597,\ c_{11} = 3.61382 - 0.89108i,\\
&c_{12} = 0.16566 - 1.3231i,\ c_{21} = -13.85122,\ c_{22} = -8.92481,\ d_{11} = 1.49544 + 0.76757i,\\
&d_{12} = -0.83811 + 0.28069i,\ d_{21} = -13.78274,\ d_{22} = 1.13355,\ e_{11} = 0.02947 - 0.01976i,\\
&e_{12} = 0.05482 - 0.70752i,\ e_{21} = 11.88788,\ e_{22} = -1.72537,\ f_{11} = -3.55352 - 0.61301i,\\
&f_{12} = -1.81478 + 4.21046i,\ f_{21} = 13.85122,\ f_{22} = 1.72537,\ g_{11} = -3.58435 + 0.5155i,\\
&g_{12} = 1.72537 - 3.34442i,\ g_{21} = -7.14128,\ g_{22} = 0.
\end{aligned} \tag{7.8}$$

This gives us $B = 1$ and $A < 0$, and therefore we have the unfolding given by Figure 3.3. The bifurcation lines for the Hopf and Cycle Blow-Up bifurcations are given by

$$\begin{aligned}
M &= \{(\mu_1, \mu_2) : \mu_2 = 2.4209\mu_1,\ \mu_1 < 0\},\\
N &= \{(\mu_1, \mu_2) : \mu_2 = 2.42092\mu_1 - 13.34186\mu_1^2 + 667.27216\mu_1^3,\ \mu_1 < 0\},
\end{aligned} \tag{7.9}$$

respectively. By taking $\mu_1 = -0.05$ and $\mu_2 = -0.2$ the point (μ_1, μ_2) lies between the curves M and N, and our work in Chapter 3 tells us that in this region there is a stable torus taking in all orbits of the system.

At first glance Figure 7.5 looks somewhat complicated in nature, but a closer inspection reveals a very unusual periodic orbit. This periodic orbit is phase-locked on the stable torus in the three dimensional system on the centre manifold. To better understand what is happening we look to Figure 7.6 where the values $x(t)$ are plotted against the independent time variable t. We can now clearly see modulated oscillation in the system; relating to the periods of oscillation along the torus in three dimensions.

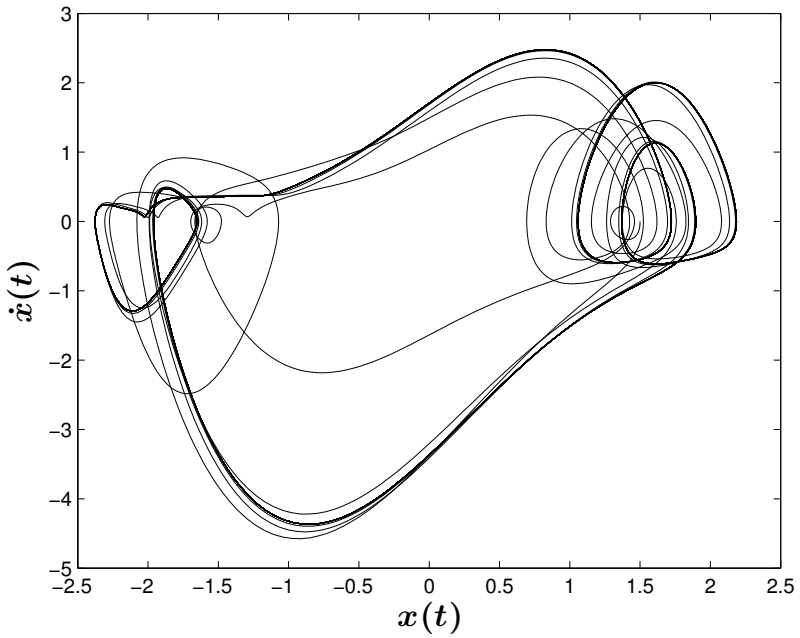

Figure 7.5: A phase-locked periodic solution occurring on the stable invariant torus on the centre manifold when $(\mu_1, \mu_2) = (-0.05, -0.2)$.

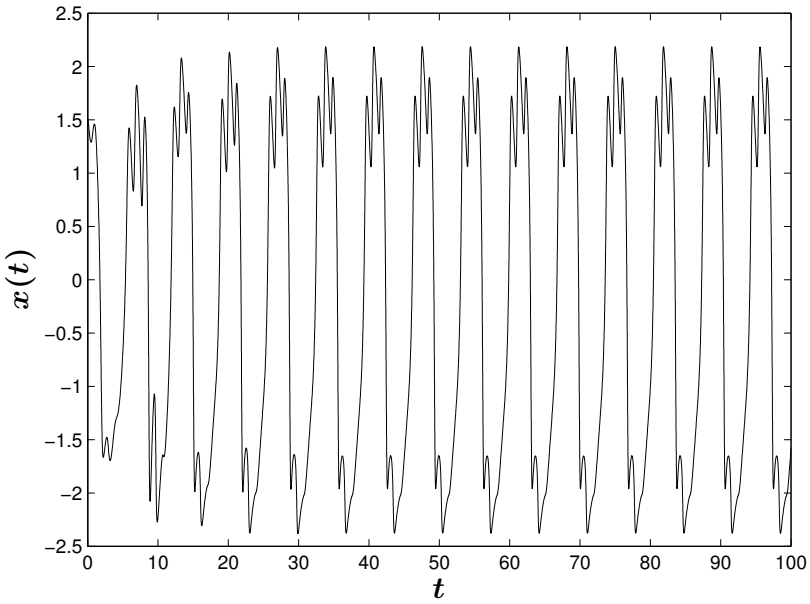

Figure 7.6: The one dimensional system showing a modulated oscillation relating to a torus on the centre manifold.

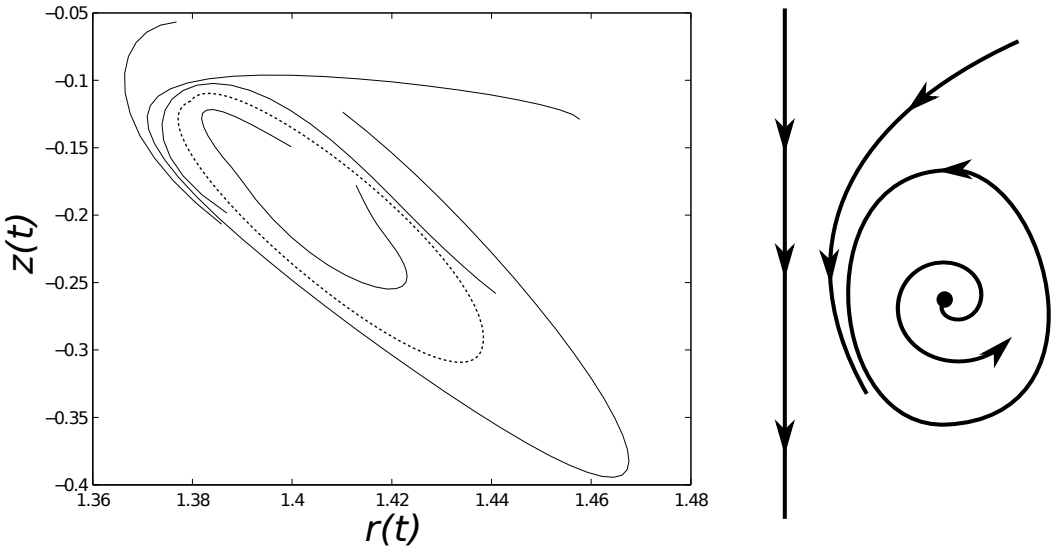

(a) (b)

Figure 7.7: (a) Projecting multiple trajectories of the system onto the centre manifold reveals a stable limit cycle in cylindrical coordinates and (b) The phase portrait predicted in Chapter 3. The limit cycle is given roughly by the dotted line.

To confirm that we are obtaining solutions that lie along an invariant torus, we use the MATLAB code given in the Appendix to project solutions on the centre manifold. Figure 7.7*a* shows these projections converging to a limit cycle in cylindrical coordinates which is given approximately by the dotted line. The bifurcation diagram predicted by our analysis of the Zero-Hopf bifurcation is given in Figure 7.7*b* to show just how accurately our theoretical and numerical results align themselves.

Although we have accurately predicted the rise of an invariant torus in our solutions, we still do not know the nature of the solutions once they are on the torus. For that reason trajectories may take many forms upon becoming attracted to the torus. That is, as our parameters move between the curves M and N, there may be bifurcations occurring on the torus itself. This could be analyzed by taking Poincare sections along a plane perpendicular to the torus and viewing the bifurcations taking

place in the related discrete dynamical system. Therefore, within the torus itself we may have stable and unstable periodic solutions.

To better illustrate this we look at another example. Take $\varepsilon = 1.2$ and $a = -0.3$ with

$$g(u_1, u_2) = au_2 + bu_1 + \frac{1}{10}u_1^2 - \frac{1}{2}u_1u_2 + \frac{1}{4}u_2^2 - \frac{1}{6}u_1^3 + \frac{1}{4}u_1^2u_2 - \frac{1}{4}u_1u_2^2 + \frac{1}{6}u_2^3. \quad (7.10)$$

Now we have $\omega_0 = 0.80623$ and $\tau_0 = 1.22344$, which gives us

$$\begin{aligned}
&a_{11} = 0.37077 - 0.74288i,\ a_{12} = -0.67123 + 0.65216i,\ a_{13} = -0.22531 - 0.29804i,\\
&a_{21} = 3.78262,\ a_{22} = 0,\ a_{23} = 1.98587,\ a_{24} = 0.37826,\ b_{11} = -0.74754 - 1.56127i,\\
&b_{12} = -0.07122 - 0.47498i,\ b_{21} = -4.60218,\ b_{22} = -0.63044,\ c_{11} = -1.93857 - 1.8442i,\\
&c_{12} = -0.84986 + 0.21608i,\ c_{21} = 11.52804,\ c_{22} = 0.91436,\ d_{11} = -0.88494 - 0.90245i,\\
&d_{12} = -0.16562 - 0.03871i,\ d_{21} = 9.3307,\ d_{22} = 0.33499,\ e_{11} = -0.21946 - 2.80922i,\\
&e_{12} = 0.05816 - 0.58682i,\ e_{21} = -1.90394,\ e_{22} = 1.11866,\ f_{11} = 0.70635 + 1.57861i,\\
&f_{12} = 1.03831 - 0.02327i,\ f_{21} = -11.52804,\ f_{22} = -1.11866,\ g_{11} = 1.71911 - 1.19195i,\\
&g_{12} = -1.11866 + 0.67254i,\ g_{21} = 2.82755,\ g_{22} = 0.
\end{aligned} \quad (7.11)$$

This gives us $B = -1$ and $A > 0$, and therefore we have the unfolding given by Figure 3.5. The bifurcation lines for the Hopf and Heteroclinic bifurcations are given by

$$\begin{aligned}
M &= \{(\mu_1, \mu_2) : \mu_2 = 2.23072\mu_1,\ \mu_1 < 0\},\\
N &= \{(\mu_1, \mu_2) : \mu_2 = 2.23072\mu_1 - 31.2522\mu_1^2 + 36.823\mu_1^3,\ \mu_1 < 0\},
\end{aligned} \quad (7.12)$$

respectively. Taking $\mu_1 = -0.02$ and $\mu_2 = -0.054$ we get that the point (μ_1, μ_2) lies between the curves M and N, and from our work in Chapter 3 we know that there is a stable torus in this region.

The phase diagram predicted in Figure 3.4 has a separatrix which tells us that depending on our initial conditions, orbits either converge to the torus or diverge

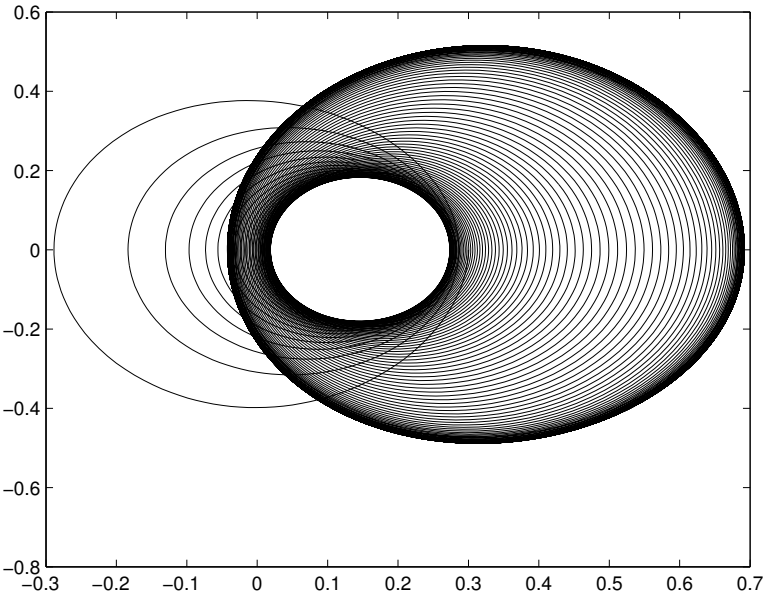

Figure 7.8: A stable and unstable limit cycle within the invariant torus when $(\mu_1, \mu_2) = (-0.02, -0.054)$.

entirely. Figure 7.8 shows one such trajectory that converges to the torus in the analogous two dimensional system. Again by projecting solutions onto the centre manifold we find a limit cycle in cylindrical coordinates confirming that the trajectory in Figure 7.8 is indeed converging to the torus. Moving from left to right in the figure we see a very quick convergence to the torus and then it appears as though the inner cycle pushes the orbits to the outer cycle in a very systematic way. It seems that there is an unstable limit cycle on the torus that pushes trajectories to a larger stable limit cycle. Not all simulations will show the unstable limit cycle, but the one presented here must have converged to the torus near the unstable cycle and once it is on the torus it thrust away and into the stable limit cycle.

The unfolding of the Zero-Hopf bifurcation leaves no indication as to what we can expect in the ways of the dynamics on the torus that is present, only that it appears through bifurcations. For this reason, the dynamics in the area between

curves M and N differs case by case and can lead to very nonintuitive results. It would be expected that Arnold tongues exist (see [1] for details) that give the period of phase-locked solutions on the torus, and therefore allow us to accurately predict the fate of trajectories after they have converged to the torus. This phase-locking on the invariant torus relates to the two periods of oscillation on the torus being related by a rational value. In the case of an irrational relation between these periods we will find that trajectories will densely cover the surface of the torus and no periodic orbits can occur in this case. Despite our claims, very little analysis has been done to further our understanding of the dynamics on the tori and therefore we are left to analyze the results as they appear in our numerical simulations.

Chapter 8

Final Thoughts

Over the course of this thesis we have seen the effect of adding a nonlinear forcing depending on a delay in feedback to the traditional van der Pol oscillator. Using methods of centre manifold reduction we have effectively reduced our study from an infinite-dimensional phase space to the three-dimensional centre manifold where the most interesting dynamics are occurring. Our theoretical work has been confirmed by numerical simulations that have also provided the reader with a visualization of the dynamics of the system.

By considering delays in not only the position of the object, but also in the velocity, we have opened up the system to dynamics that were not possible with only the delay in position. That is, the system can now attain all four unfoldings given in Chapter 3 for the Zero-Hopf bifurcation, and therefore gives us a richer system that depends greatly on the initial values in the system. We see that only a few variables defined in the system can greatly affect its dynamics and give way to some very interesting phenomena.

One of the most interesting aspects of the study presented in this thesis is the numerical projection onto the centre manifold using the theoretical techniques given in Chapter 4. The code for this procedure is given in the appendix to provide the

reader with the tools to conduct their own experiments on delay differential equations. This numerical projecting technique has allowed us to draw the connection between the given DDE and the three-dimensional phase portraits given by the Zero-Hopf bifurcation, allowing the reader to easily visualize the dynamics of the system without any manual computation.

The work in this thesis has essentially made the work of Jiang and Wei a special case of the broader system studied here. In [19] mathematicians Wang and Wu studied the Zero-Hopf bifurcation occurring in Jiang and Wei's system and found that only two of the four possible unfoldings could be obtained. We now see that the added delay in velocity has allowed us to obtain all four of the unfoldings, and therefore allowing the system to take on much richer dynamics. In short, system (1.5) is the most general case for delayed forcing studied to date in the van der Pol oscillator. The results here now give that all other delayed forcing studied in the van der Pol oscillator is a special case of the work in this thesis, while also expanding the dynamics of the system and allowing for much more interesting results.

Moving forward, it would be very interesting to observe the behaviour of the other bifurcations that are given in Theorem 2.1. Since we have seen the effects on the Zero-Hopf bifurcation by adding a delay in velocity, it might be worth investigating the behaviour of the other bifurcations under the same conditions. In Chapter 2 we also saw that a quadruple zero eigenvalue is possible under certain conditions, which is a bifurcation that is unique to the forcing on the equation given in this thesis. This bifurcation may also lead us to many very interesting dynamics and peculiar results that could be of interest in a physical setting, but as of the completion of this thesis there is little known about such a bifurcation.

This work also leaves the reader wondering what effects adding delays in higher order derivatives of the solution to the forcing component will have on the system. This work has only touched the surface as to what can be expected in a system with a delay in forcing and possibilities left to explore seem endless. For these reasons, and

many more, the study of delay differential equations becomes increasingly important for mathematicians to model the world around us.

Appendix A

Calculation of the terms h_{ijk}

Lemma A.1. *Equation* (5.35) *gives us*

$$
\begin{aligned}
h_{200}^{(1)}(-1) = {} & \frac{e^{-2i\omega_0\tau_0}}{2\omega_0}(g_{u_1u_1}(0,0) + 2i\omega_0 g_{u_1u_2}(0,0) - \omega_0^2 g_{u_2u_2}(0,0))\Big[\bar{D}\bar{\sigma}(ie^{2i\omega_0\tau_0} + a\omega_0 \\
& - a\omega_0 e^{-3i\omega_0\tau_0} + a\omega_0 e^{2i\omega_0\tau_0} + \varepsilon\omega_0 e^{2i\omega_0\tau_0} - 7ie^{2i\omega_0\tau_0} + 3ia^2 e^{2i\omega_0\tau_0}) \\
& + \frac{1}{6}D\sigma(2ie^{2i\omega_0\tau_0} - 2ie^{5i\omega_0\tau_0} + 6a\omega_0 + 2a\omega_0 e^{5i\omega_0\tau_0} + 2ie^{5i\omega_0\tau_0} + 6ia^2 e^{2i\omega_0\tau_0} \\
& - 2a\omega_0 e^{2i\omega_0\tau_0} + 6\varepsilon\omega_0 e^{2i\omega_0\tau_0} + 6i\varepsilon^2\omega_0 e^{2i\omega_0\tau_0} - 14ie^{2i\omega_0\tau_0}) + \frac{1}{6}D_1(-3ie^{2i\omega_0\tau_0} \\
& + 3ie^{4i\omega_0\tau_0} - 6a\omega_0 - 3ie^{4i\omega_0\tau_0} - 6\varepsilon\omega_0 e^{2i\omega_0\tau_0} - 12ia^2 e^{2i\omega_0\tau_0} - 12i\varepsilon^2 e^{2i\omega_0\tau_0} \\
& + 27ie^{2i\omega_0\tau_0}) + 6\omega_0 e^{2i\omega_0\tau_0}\Big], \\
h_{200}^{(2)}(-1) = {} & \frac{-e^{-2i\omega_0\tau_0}}{2\omega_0}(g_{u_1u_1}(0,0) + 2i\omega_0 g_{u_1u_2}(0,0) - \omega_0^2 g_{u_2u_2}(0,0))\Big[\bar{D}\bar{\sigma}(-8e^{2i\omega_0\tau_0} \\
& + e^{3i\omega_0\tau_0} + 1 - 2ia\omega_0 e^{2i\omega_0\tau_0} + 2e^{3i\omega_0\tau_0} + 2ia\omega_0 e^{3i\omega_0\tau_0} + 2\varepsilon^2 e^{2i\omega_0\tau_0} + 2a^2 e^{2i\omega_0\tau_0}) \\
& + D\sigma(\frac{8}{3}e^{2i\omega_0\tau_0} + 1 + \frac{1}{3}e^{5i\omega_0\tau_0} + \frac{2}{3}ia\omega_0 e^{2i\omega_0\tau_0} - \frac{2}{3}ia\omega_0 e^{5i\omega_0\tau_0} - 2a^2 e^{2i\omega_0\tau_0} \\
& - 2\varepsilon^2 e^{2i\omega_0\tau_0}) + D_1(-1 - e^{4i\omega_0\tau_0} + 2e^{2i\omega_0\tau_0}) - 2i\omega_0 e^{2i\omega_0\tau_0}\Big]
\end{aligned}
\tag{A.1}
$$

Proof: Applying the integrating factor $e^{-2i\omega_0\tau_0}$ to equation (5.35), we obtain

$$h_{200}(\theta) = e^{2i\omega_0\tau_0}\int_0^\theta e^{-2i\omega_0\tau_0}\Phi(t)\Psi(0)A_{200}dt + ce^{2i\omega_0\tau_0} \tag{A.2}$$

where $c \in \mathbb{C}^2$ is a constant and now we have

$$\dot{h}_{200}(0) = \Phi(0)\Psi(0)A_{200} + 2i\omega_0\tau_0 c. \tag{A.3}$$

Now using the definition of the operator L we get

$$L(h_{200}) = \mathbb{B}e^{-2i\omega_0\tau_0}\int_0^{-1} e^{-2i\omega_0\tau_0}\Phi(t)\Psi(0)A_{200}dt + L(e^{2i\omega_0\tau_0})c, \tag{A.4}$$

and from the second equation of (5.35) we have

$$(2i\omega_0\tau_0 I - L(e^{2i\omega_0\tau_0}))c = -(\Phi(0)\Psi(0) - I)A_{200} - \mathbb{B}\int_{-1}^0 e^{-2i\omega_0\tau_0}\Phi(t)\Psi(0)A_{200}dt. \tag{A.5}$$

This gives us

$$c = (2i\omega_0\tau_0 I - L(e^{2i\omega_0\tau_0})^{-1}\bigg[-(\Phi(0)\Psi(0) - I)A_{200} - \mathbb{B}\int_{-1}^0 e^{-2i\omega_0\tau_0}\Phi(t)\Psi(0)A_{200}dt\bigg]. \tag{A.6}$$

Therefore, after long computation we arrive at the desired expression for $h_{200}(-1)$. ∎

Lemma A.2. *Equation* (5.36) *gives us*

$$\begin{aligned}
h_{101}^{(1)}(-1) = \frac{e^{-i\omega_0\tau_0}(g_{u_1u_1}(0,0) + i\omega_0 g_{u_1u_2}(0,0))}{2a\omega_0(1+i\omega_0)}\Big[&\bar{D}\bar{\sigma}(2\tau_0 e^{-i\omega_0\tau_0} - 2\varepsilon\omega_0 - 2ia\omega_0\tau_0 e^{-i\omega_0\tau_0} \\
&- 2i\varepsilon^2 a\tau_0 e^{-i\omega_0\tau_0} - 2ae^{-i\omega_0\tau_0} - 4i\varepsilon^2 + 4ia^2 + 8i + 2ia^3\tau_0 e^{-i\omega_0\tau_0} + 4ia\tau_0 e^{-i\omega_0\tau_0} \\
&- 2a\omega_0\tau_0 e^{-i\omega_0\tau_0}) + D\sigma(-2\varepsilon\omega_0 + ie^{-i\omega_0\tau_0} - ie^{i\omega_0\tau_0} - 2a\omega_0 e^{i\omega_0\tau_0} + iae^{i\omega_0\tau_0} \\
&- iae^{-i\omega_0\tau_0}) + D_1(-2a\omega_0 e^{-i\omega_0\tau_0} + 2iae^{-i\omega_0\tau_0} + 2\varepsilon\omega_0 + 2a\omega_0 + 2ae^{-i\omega_0\tau_0} - 2ia \\
&- 2ia^2 + 2i\varepsilon^2 - 2i) - 2\omega_0\Big], \\
h_{101}^{(2)}(-1) = \frac{-e^{-i\omega_0\tau_0}(g_{u_1u_1}(0,0) + i\omega_0 g_{u_1u_2}(0,0))}{a(1+i\omega_0)}\Big[&\bar{D}\bar{\sigma}(-2a\omega_0^2\tau_0 e^{-i\omega_0\tau_0} + 6 - 2e^{-i\omega_0\tau_0} \\
&- 2\varepsilon^2 + 2a^2 - 2i\omega_0\tau_0 e^{-i\omega_0\tau_0} + 4a\tau_0 e^{-i\omega_0\tau_0} - 2\varepsilon^2 a\tau_0 e^{-i\omega_0\tau_0} + 2a^3\tau_0 e^{-i\omega_0\tau_0} \\
&+ 2ia\omega_0\tau_0 e^{-i\omega_0\tau_0}) + D\sigma(-ae^{i\omega_0\tau_0} + ae^{-i\omega_0\tau_0} - 2 - e^{-i\omega_0\tau_0} + 2\varepsilon^2 - 2a^2 - e^{i\omega_0\tau_0}) \\
&+ 2i\omega_0\Big].
\end{aligned} \tag{A.7}$$

Proof: Using the integrating factor $e^{-i\omega_0\tau_0}$, equation (5.36) gives us that

$$h_{101}(\theta) = e^{i\omega_0\tau_0}\int_0^\theta e^{-i\omega_0\tau_0}\Phi(t)\Psi(0)A_{101}dt + ce^{i\omega_0\tau_0} \tag{A.8}$$

where $c \in \mathbb{C}^2$ is a constant. Differentiating with respect to theta now gives

$$\dot{h}_{101}(0) = \Phi(0)\Psi(0)A_{101} + i\omega_0\tau_0 c. \tag{A.9}$$

From the definition of the operator L we get

$$L(h_{101}) = \mathbb{B}e^{-i\omega_0\tau_0}\int_0^{-1} e^{-i\omega_0\tau_0}\Phi(t)\Psi(0)A_{101}dt + L(e^{i\omega_0\tau_0})c, \tag{A.10}$$

and from the second equation of (5.36) we have

$$(i\omega_0\tau_0 I - L(e^{i\omega_0\tau_0}))c = -(\Phi(0)\Psi(0) - I)A_{101} - \mathbb{B}\int_{-1}^0 e^{-i\omega_0\tau_0}\Phi(t)\Psi(0)A_{101}dt. \tag{A.11}$$

This gives us

$$c = (i\omega_0\tau_0 I - L(e^{i\omega_0\tau_0})^{-1}\Big[-(\Phi(0)\Psi(0) - I)A_{101} - \mathbb{B}\int_{-1}^0 e^{-i\omega_0\tau_0}\Phi(t)\Psi(0)A_{101}dt\Big]. \tag{A.12}$$

Therefore, after long computation we get the desired expression for $h_{101}(-1)$. ∎

Lemma A.3. *Equation* (5.37) *gives us*

$$\begin{aligned} h_{110}^{(1)}(-1) &= -2(g_{u_1u_1}(0,0)+\omega_0^2 g_{u_2u_2}(0,0))\Big[\frac{2}{\omega_0}(\mathrm{Im}[D\sigma(1-e^{i\omega_0\tau_0})]) - \tau_0 D_1 \\ &\quad + \frac{1}{\varepsilon+a}(2\mathrm{Re}[D\sigma]-D_1)\Big], \\ h_{110}^{(2)}(-1) &= -2(g_{u_1u_1}(0,0)+\omega_0^2 g_{u_2u_2}(0,0))\big[2\mathrm{Re}[D\sigma(1-e^{i\omega_0\tau_0})] \\ &\quad + (\varepsilon+a)(2\mathrm{Re}[D\sigma]-D_1)\big]. \end{aligned} \tag{A.13}$$

Proof: By integrating the first equation we get

$$h_{110}(\theta) = \int_0^\theta \Phi(t)\Psi(0)A_{110}dt + c. \tag{A.14}$$

Then differentiating with respect to theta we get

$$\dot{h}_{110}(0) = \Phi(0)\Psi(0)A_{110}, \tag{A.15}$$

and

$$L(h_{110}) = \mathbb{B}\int_0^{-1} \Phi(t)\Psi(0)A_{110}dt + L(1)c. \tag{A.16}$$

From the second equation we get

$$L(1)c = -(\Phi(0)\Psi(0)-I)A_{110} - \mathbb{B}\int_{-1}^0 \Phi(t)\Psi(0)A_{110}dt. \tag{A.17}$$

Call the right side of this equation b_1. Then calculation shows that

$$b_1 = -2\tau_0(g_{u_1u_1}(0,0)+\omega_0^2 g_{u_2u_2}(0,0))(2\mathrm{Re}[D\sigma]-D_1)\begin{pmatrix}1\\ \varepsilon+a\end{pmatrix}. \tag{A.18}$$

Since $L(1) = \mathbb{A}+\mathbb{B}$ is not an invertible matrix we use Kuznetsov's method presented in [10]. From the facts

$$\begin{aligned} &L(1)\varphi_2(0) = 0, \quad \psi_2(0)L(1) = 0, \\ &(D_1^{-1}(\varepsilon+a)^{-1}\psi_2(0),\varphi_2(0)) = 1, \quad (D_1^{-1}(\varepsilon+a)^{-1}\psi_2(0),b_1) = 0, \end{aligned} \tag{A.19}$$

we may solve the bordered system

$$\begin{pmatrix} L(1) & \varphi_2(0) \\ D_1^{-1}(\varepsilon+a)^{-1}\psi_2(0) & 0 \end{pmatrix} \begin{pmatrix} w \\ u \end{pmatrix} = \begin{pmatrix} b_1 \\ 0 \end{pmatrix}. \tag{A.20}$$

We find a unique solution $w = L(1)^{INV}b_1$ to the system. By setting $c = L(1)^{INV}b_1$, and using this c we obtain the desired equation for $h_{110}(-1)$, as needed. ∎

Lemma A.4. *Equation* (5.38) *gives us*

$$\begin{aligned} h_{002}^{(1)}(-1) &= -g_{u_1u_1}(0,0)\left[\frac{2}{\omega_0}(\mathrm{Im}[D\sigma(1-e^{i\omega_0\tau_0})]) - \tau_0 D_1 + \frac{1}{\varepsilon+a}(2\mathrm{Re}[D\sigma]-D_1)\right], \\ h_{002}^{(2)}(-1) &= -g_{u_1u_1}(0,0)\big[2\mathrm{Re}[D\sigma(1-e^{i\omega_0\tau_0})] + (\varepsilon+a)(2\mathrm{Re}[D\sigma]-D_1)\big]. \end{aligned} \tag{A.21}$$

Proof: By integrating the first equation we get

$$h_{002}(\theta) = \int_0^\theta \Phi(t)\Psi(0)A_{002}dt + c. \tag{A.22}$$

Then differentiating with respect to theta we get

$$\dot{h}_{002}(0) = \Phi(0)\Psi(0)A_{002}, \tag{A.23}$$

and

$$L(h_{002}) = \mathbb{B}\int_0^{-1} \Phi(t)\Psi(0)A_{002}dt + L(1)c. \tag{A.24}$$

From the second equation we get

$$L(1)c = -(\Phi(0)\Psi(0)-I)A_{002} - \mathbb{B}\int_{-1}^0 \Phi(t)\Psi(0)A_{002}dt. \tag{A.25}$$

Call the right side of this equation b_2. Then calculation shows that

$$b_2 = -\tau_0(g_{u_1u_1}(0,0)(2\mathrm{Re}[D\sigma]-D_1)\begin{pmatrix} 1 \\ \varepsilon+a \end{pmatrix}. \tag{A.26}$$

Again, $L(1) = \mathbb{A} + \mathbb{B}$ is not an invertible matrix so we create a bordered system using the following,

$$\begin{aligned} &L(1)\varphi_2(0) = 0, \quad \psi_2(0)L(1) = 0, \\ &(D_1^{-1}(\varepsilon + a)^{-1}\psi_2(0), \varphi_2(0)) = 1, \quad (D_1^{-1}(\varepsilon + a)^{-1}\psi_2(0), b_2) = 0. \end{aligned} \tag{A.27}$$

This bordered system now becomes

$$\begin{pmatrix} L(1) & \varphi_2(0) \\ D_1^{-1}(\varepsilon + a)^{-1}\psi_2(0) & 0 \end{pmatrix} \begin{pmatrix} w \\ u \end{pmatrix} = \begin{pmatrix} b_2 \\ 0 \end{pmatrix}. \tag{A.28}$$

As in the proof of Lemma $A.3$, we find a unique solution $w = L(1)^{INV} b_2$ to the system. Setting $c = L(1)^{INV} b_2$, and we can now find $h_{002}(-1)$. ∎

Appendix B

MATLAB Code

Here we provide the MATLAB code for the numerical centre projection program detailed in Chapter 7. We utilize the methods presented in Chapter 4 to reduce the infinite dimensional delay-differential equation to an equivalent three dimensional ordinary differential equation on the centre manifold. Using the bilinear form given in equation (5.11) we decompose trajectories of the delay equation to obtain a trajectory on the centre manifold. By running this program with many different initial conditions in the delay equation we are able to create our own phase diagrams and compare them with those presented in Chapter 3. Examples of such diagrams are given in Figures 7.2a, 7.4a and 7.7a.

```
function [rsmooth,zsmooth] = CentreProjection(r0,z0, tfinal, eps, a)


% CentreProjection: A numerical centre projection function
%
% Syntax:
%   [rsmooth,zsmooth] = CentreProjection(r0,z0, tfinal, eps, a)
%
% Inputs:
```

```
%   r0, z0: Initial values for cylindrical starting position.
%   tfinal: Number of iterations to be done by DDE simulator
%   eps, a: Variables from van der Pol oscillator
%
% Output
%   [rsmooth, zsmooth]: A two dimensional vector of cylindrical
%                       coordinates.
%
% Example,
%   [rsmooth,zsmooth] = CentreProjection(0.1,-0.1, 100, 1, 0.2);
%   plot(rsmooth,zsmooth)
%
% The CentreProjection function projects solution trajectories of the
% delayed van der Pol oscillator onto the three dimensional centre
% manifold. Solutions are given in cylindrical coordinates and are
% projected using the Bilinear Form from chapter 5. DDE simulations are
% obtained using the built in MATLAB function dde23.
%
% Output utilizes supsmu.m, a numerical smoothing program created by
% Douglas M. Schwarz. It is publicly available on the MATLAB
% Central file exchange. The algonrithm uses Friedman's supersmoother
% algorithm to produce smoother and more accurate results.
%

%Variable Declarations
t = 0;
X = zeros(3,tfinal);
r = zeros(1,tfinal);
```

```
z = zeros(1,tfinal);

%Constants
w0 = sqrt(2 - eps^2 + a^2);
tau0 = (1/w0)*acos((1-((1+eps*a)*(w0^2)))/((a^2)*(w0^2)+1));
sigma = -1i*w0/(exp(1i*w0*tau0)-1);
sigmaC = conj(sigma);
DC = 1/(1+1i*sigmaC*w0 + tau0*sigmaC*exp(-1i*w0*tau0)*(1+1i*a*w0));
D = conj(DC);
D1 = 1/(eps + a - tau0);

%DDE Simulator
options = ddeset('RelTol',1e-5,'InitialStep',0.01,'MaxStep',0.005);
sol = dde23('ddefun',1,'history',[0 tfinal],options,r0,z0);

%The Bilinear Form
while t < tfinal
    t0 = find(sol.x-t >= 0,1);
    t1 = find(sol.x-t-1 >= 0,1);
    f = zeros(3,t1-t0+1);

    initialBilinear = [DC*sol.y(1,t1) + DC*sigmaC*sol.y(2,t1);
     D*sol.y(1,t1) + D*sigma*sol.y(2,t1); D1*(eps + a)*sol.y(1,t1) -
D1*sol.y(2,t1)];
    index = t0;

    while index <= t1
        xi = sol.x(index)-t;
```

```
        f(:,index-t0+1) = [tau0*DC*sigmaC*exp(-1i*w0*tau0*xi)*
        (sol.y(1,index) + a*sol.y(2,index));
        tau0*D*sigma*exp(1i*w0*tau0*xi)*(sol.y(1,index)
        + a*sol.y(2,index)); -tau0*D1*(sol.y(1,index)
        + a*sol.y(2,index))];
        index = index+1;
    end

    intpoints = sol.x(t0:t1) - t -1;
    integral1 = trapz(intpoints,f(1,:));
    integral2 = trapz(intpoints,f(2,:));
    integral3 = trapz(intpoints,f(3,:));

    t = t+1;
    X(:,t) = initialBilinear + [integral1; integral2; integral3];
end

%Conversion from Complex to Real Values
realPart = (X(1,:) + X(2,:))/2;
imaginaryPart = (X(1,:) - X(2,:))/2i;

%Conversion to Cylindrical Coordinates
r = sqrt(realPart.^2 + imaginaryPart.^2);
z = X(3,:);

%Smoothing of the values
l = 1:length(r);
rsmooth = supsmu(l,r);
```

```
zsmooth = supsmu(l,z);
```

Bibliography

[1] D.K. Arrowhead, C.M. Place, *An Introduction to Dynamical Systems*, Cambridge University Press, New York, 1990.

[2] F. M. Atay, Van der Pol's oscillator under delayed feedback, *J. Sound and Vibration* **218**, (1998) 333-339.

[3] J. H. E. Cartwright, V. M. Eguiluz, E. Hernandez-Garcia, O. Piro, Dynamics of elastic excitable media, *Int. J. Bifurcation and Chaos* **9** (1999) 2197-2202.

[4] T. Faria, L.T. Magalhães, Normal forms for retarted functional differential equations with parameters and application to Hopf bifurcation, *J. Differential Equations* **122** (1995) 181-224.

[5] T. Faria, L.T. Magalhães, Normal forms for retarted functional differential equations and applications to Bogdanov-Takens singularity, *J. Differential Equations* **122** (1995) 201-224.

[6] J. Guckenheimer, P. Holmes, *Nonlinear Oscillations, Dynamical Systems, and Bifurcation of Vector Fields*, Springer-Verlag, New York, 1983.

[7] J. K. Hale, S. M. Verduyn Lunel, *Introduction to Functional Differential Equations*, Springer-Verlag, New York, 1993.

[8] W. Jiang, Y. Yuan, Bogdanov-Takens singularity in Van der Pol's oscillator with delayed feedback, *Physica D* **227** (2007) 149-161

[9] B. Z. Kaplan, I. Gabay, G. Sarafian, D. Sarafian, Biological applications of the Filtered Van der Pol oscillator, *Journal of the Franklin Institute* **345** (2008) 226-232.

[10] Y. A. Kuznetsov, *Elements of Applied Bifurcation Theory*, Springer-Verlag, New York, 2004, 3rd ed.

[11] W. F. Langford, Periodic and steady-state mode interactions lead to tori, *J. Applied Mathematics* **37** (1979) 22-48.

[12] J.C.F. de Oliveira, Oscillations in a van der Pol equation with delayed argument, *J. Mathematical Analysis and Applications* **275** (2002) 789-803.

[13] L. P. Shayer, S. A. Campbell, Stability, bifurcation, and multi stability in a system of two coupled neurone with multiple time delays, *J. Applied Mathematics* **61** (2000) 673-700.

[14] E. Stone, S. A. Campbell, Stability and bifurcation analysis of a nonlinear DDE model for drilling, *J. Nonlinear Science* **14** (2004) 27-57.

[15] B. van der Pol, A theory of the amplitude of free and forced triode vibrations, *Radio Review* **1** (1920) 754-762.

[16] J. Wei, W. Jiang, Stability and bifurcation analysis in Van der Pol's oscillator with delayed feedback, *J. Sound Vibration* **283** (2005) 80-819.

[17] J. Wei, W. Jiang, Bifurcation analysis in van der Pol's oscillator with delayed feedback, *J. Computational and Applied Mathematics* **213** (2008) 604-615.

[18] S. Wiggins, *Introduction to Applied Nonlinear Dynamical Systems and Chaos*, Springer-Verlag, New York, 2003.

[19] X. Wu, L. Wang, Zero-Hopf bifurcation for van der Pol's oscillator with delayed feedback *J. Computational and Applied Mathematics* **235** (2011) 2586-2602